Modulation of Metastable Metal-Semiconductor Junctions

by

Lixia Zhu

M.Eng., Kyungwon University, 2011
B.Eng., Shandong University, 2009

Thesis Submitted in Partial Fulfillment of the

Requirements for the Degree of

Master of Science

in the

Department of Chemistry

Faculty of Science

SIMON FRASER UNIVERSITY

Fall 2014

Approval

Name: **Lixia Zhu**

Degree: **Master of Science (Chemistry)**

Title of Thesis: ***Modulation of Metastable Metal-Semiconductor Junctions***

Examining Committee: **Chair:** **Dr. Michael H. Eikerling**
Professor, Department of Chemistry, SFU

Dr. Hua-Zhong Yu
Senior Supervisor
Professor, Department of Chemistry, SFU

Dr. Byron D. Gates
Supervisor
Associate Professor, Department of Chemistry, SFU

Dr. Eldon Emberly
Supervisor
Associate Professor, Department of Physics, SFU

Dr. Karen Kavanagh
External Examiner
Professor
Department or Physics, SFU

Date Defended/Approved: September 26, 2014

Partial Copyright Licence

Abstract

The feasibility of modulating the electrical properties of metal-semiconductor (MS) junctions was examined via the preparation of self-assembled monolayers (SAMs) at the interface. In this thesis, metal-monolayer-semiconductor junctions were prepared using a hanging mercury (Hg) drop electrode in contact with an oxide-free silicon substrate (H-Si≡), where the mercury drop was subsequently modified with alkanethiolate SAMs. It has been demonstrated that the electrical properties of an Hg-S-C18|H-Si≡ junction can be tuned from rectifying to ohmic or vice versa by manual manipulation of the size and shape of the Hg drop. Evaluation of the rectification ratio (R), ideality factor (η) and barrier height ($q\phi_{eff}$) enables the determination of the threshold value of the surface area change of the mercury contact. In addition, the effect of variation of the alkyl chain length of the alkanethiolate SAMs on the Hg electrode was studied. Both $q\phi_{eff}$ and R were found to depend on the alkyl chain length and changed gradually upon aging. This augment the potential for molecularly tuning the electrical properties of classical MS junctions without complicated materials assembly or device fabrication.

Keywords: Mercury, Self-assembled monolayer (SAM), Hydrogen-terminated silicon, Ohmic, Rectifying

Dedication

To my family and friends!

Acknowledgements

Firstly, I would like to take this opportunity to express my profound gratitude and deep appreciation to my senior supervisor, Dr. Hua-Zhong (Hogan) Yu who provided me the opportunity to study in his group. With his exemplary guidance, monitoring, and support throughout the years, I have improved myself a lot by learning chemistry and proceed a long way in the journey of life on which I am about to embark.

I would also like to take this opportunity to express a deep sense of gratitude to Dr. Byron Gates and Dr. Eldon Emberly for being my committee members; their advice and suggestions have been tremendously helpful to my studies. I also give thanks to Dr. Michael Eikerling and Dr. Karen Kavanagh for taking the time to serve as the chair and external examiner at my defence.

In addition, I would like to thank Dr. Eberhard Kiehlmann for proofreading my thesis. I thank Dr. Richard Popoff for training me and giving me helpful advice on my research. I also thank Michael Wang (Gates Lab) for training on the x-ray photoelectron spectrometer. I am very thankful to the past and present members of the Yu laboratory for their friendship and support.

Finally, I would like to express my deepest thankfulness to my family for their unconditional support and encouragement.

Table of Contents

Approval ii
Partial Copyright Licence iii
Abstract iv
Dedication v
Acknowledgements vi
Table of Contents vii
List of Tables ix
List of Figures x
List of Acronyms xiii

1. Introduction 1
1.1. Metal-Semiconductor (MS) Junctions 2
1.1.1. History and Applications 2
1.1.2. Electrical Properties of MS Junctions 2
1.2. Self-Assembled Monolayers (SAMs) 7
1.2.1. SAMs on Hg 10
1.2.2. SAMs on Si 11
1.3. Metal-Monolayer-Semiconductor Junctions 13
1.3.1. Hg | Monolayer-Si≡ (R-Si≡) Junctions 13
1.3.2. Hg-Monolayer|H-Si≡ Junctions 14
1.4. Objectives of This Thesis 15

2. Experimental Section 16
2.1. Materials and Reagents 16
2.2. Sample Preparation 16
2.2.1. Preparation of Hydrogen-terminated Silicon (H-Si≡) 16
2.2.2. Preparation of a Hg-SAM|H-Si≡ Junction 17
2.2.3. Formation of a Hg|R-Si≡ Junction 18
2.3. Solid-State Electrical Measurements 19
2.4. Electrochemical Studies of SAMs on Hg 20
2.5. Formation of Fullerene Monolayers on Si Surface 21

3. Results and Discussion 22
3.1. Electrical Properties of Hg-S-C18|H-Si≡ Junctions 22
3.1.1. Volume Expansion of the Hg Contact 22
3.1.2. Deformation of the Hg Contact 27
3.1.3. *Electrical Properties of Hg|C12-S-Si≡ Junctions* 31
3.1.4. Electrochemical Studies of C18SH SAM on Hg 32
3.1.5. Hypothetical Structural Change of SAMs on Hg Contact 33
3.2. Electrical Properties of Hg-SAM|H-Si≡ Junctions with Alkanethiols of Different Chain Lengths 35

3.2.1. Electrical Behavior of Junctions Formed with Short Chain Alkanethiols 35
3.2.2. Electrical Behavior of Junctions with Long Chain Alkanethiols 39
3.2.3. Discussion 41
3.3. Preliminary Studies of Hg|fullerene-Si≡ Junctions 44

4. Conclusions and Future Work 49
4.1. Conclusions 49
4.2. Future Work 50

References 52

Appendices 60
Appendix A. Safe Handling Procedure of "Piranha" Cleaning 61
Appendix B. Safe Handling Procedure of Ammonium Fluoride 40% Solution 62
Appendix C. Electrical Properties for Hg-S-C18|H-Si≡ Junctions: Reproducibility 65
Appendix D. Electrical Properties for Hg|C12-S-Si≡ Junctions: Reproducibility 66

List of Tables

Table 3.1 Volume expansion of Hg drop.....25

Table 3.2 Deformation of Hg drop 28

List of Figures

Figure 1.1 Energy-band diagram of a metal and semiconductor (a) before contact and (b) after contact. E_F is the Fermi level and E_C and E_V are the conduction band and the valence band of the semiconductor. $q\phi_M$, $q\phi_S$, $q\chi_S$ and $q\phi_n$ are the metal work function, the semiconductor work function, the electron affinity of the semiconductor and the energy difference between E_C and E_F, respectively. 4

Figure 1.2 Energy-band diagram of a MS junction under (a) forward bias and (b) reverse bias. V_F is the magnitude of the forward bias while V_R is the magnitude of the reverse bias. 6

Figure 1.3 Idealized representation of a self-assembled monolayer (SAM) on a solid substrate. 8

Figure 1.4 Mechanism of terminal alkene reaction with H-Si≡ via radical initiation. 12

Figure 1.5 Schematic illustration of the electrical properties of a Hg|H-Si≡ junction vs. a Hg|monolayer-Si≡ junction. 14

Figure 2.1 Schematic illustration of the preparation of H-Si≡ 16

Figure 2.2 Schematic view of the formation of a Hg-S-Cn|H-Si≡ junction. 18

Figure 2.3 Formation of a Hg|R-Si≡ junction. The monolayer-modified Si was cleaned with 2% TFA in THF, sonication in dichloromethane for 30 s and then dried by a stream of N_2. 18

Figure 2.4 Schematic view of the apparatus used to measure current density versus voltage properties: (a) a Hg-SAM|H-Si≡ junction; (b) a Hg|R-Si ≡ junction. 19

Figure 2.5 Electrochemical setup with the SAM modified Hg drop as the working electrode. (A) Ag|AgCl|3M NaCl reference electrode, (B) Hg drop modified with an alkanethiolate SAM, (C) platinum counter electrode, (D) tungsten wire connecting the Hg working electrode, (E) the gas-tight syringe, and (F) a glass cell of approximately 40 mL volume, (P) potentiostat. 20

Figure 2.6 Immobilization of C_{60} on hydrogen-terminated Si surface. 21

Figure 3.1 (a) Representative current-density vs. voltage (*J*-*V*) plots of a Hg-S-C18|H-Si≡ junction upon enlarging the Hg drop volume. (b) Rectification ratio (*R*) vs. surface area ratio, and (c) barrier height $q\phi_{eff}$ (black circles) and ideality factor η (red squares) vs. A/A_0. 23

Figure 3.2 Schematic view of the spherical shape of a Hg drop upon forming contact with H-Si≡ as initially prepared and after volume expansion. (The schematic view is around 25 times larger than the real size of Hg drop.)....24

Figure 3.3 Calculation of the effective barrier heights and ideality factor from the linear fitting of the J-V curves: plot of ln[*J*/(1-*exp*(-*qV*/*kT*))] versus *V* for a Hg-S-C18|H-Si≡ junction as prepared. 26

Figure 3.4 Schematic view of the oblate shape of a Hg drop upon pressing down the syringe. (The schematic view is around 25 times larger than the real size of Hg drop.) 28

Figure 3.5 (a) Representative current density vs. voltage (*J*-*V*) plots for Hg-S-C18/H-Si≡ junction upon deforming the Hg drop. (b) Rectification ratio (*R*) and (c) barrier height $q\phi_{eff}$ upon changing the shape of the Hg drop. Stage 0: freshly made Hg-S-C18|H-Si≡ junction; stage 1: “depressed” drop; stage 2: “released” drop. 29

Figure 3.6 Representative current density vs. voltage (*J*-*V*) plots for Hg|C12-S-Si≡ junction upon enlarging the Hg drop. These junctions showed no changes in their electrical behaviour during both volume expansion and deformation of the Hg contact. 31

Figure 3.7 Cyclic voltammograms of 5 mM $Ru(NH_3)_6^{3+}$ on a C18 SAM-modified Hg drop before (black line) and after 11% increase of the surface area (red line). The scan rate was 50 mV/s, and the supporting electrolyte was 0.1 M KCl. 32

Figure 3.8 Schematic view of the potential structural changes in a C18 SAM on Hg (as top electrode) in contact with H-Si≡: (a) a defect-free junction; (b) alkyl chains tilted and small bare spots created when increasing the surface area of the Hg drop; (c) direct contact between bare Hg and H-Si≡ upon further increasing the surface area. 34

Figure 3.9 Variation of current density-voltage (*J*-*V*) curves of Hg-S-Cn|H-Si≡ junctions (n = 10, 11, 12) with time. Current density under reverse bias initially decreases with time, as indicated by the black arrow. After longer periods of time, the current densities under both reverse and forward bias increase until the *J*-*V* curves become symmetric. 36

Figure 3.10 Variation of the rectification ratio (*R*) as function of time for the Hg-S-Cn|H-Si≡ (n=10, 11, 12) junctions. 37

Figure 3.11 (a) Barrier height ($q\phi_{eff}$) (circles) and (b) Ideality factor (η) (squares) as function of time for the alkanethiols junctions prepared from short chain. 38

Figure 3.12 Current density-voltage (*J-V*) curves of various Hg-S-Cn|H-Si≡ (n=14, 16, 18) junctions. Current density under reverse bias decreases with time, as indicated by the black arrow. 39

Figure 3.13 Rectification ratio (*R*) as function of time for the long-chain Hg-S-Cn|H-Si≡ junctions. 40

Figure 3.14 (a) Barrier hight ($q\phi_{eff}$) (circles). (b) Ideality factor (η) (squares) as function of time for the alkanethiols junctions prepared from long chain. 41

Figure 3.15 (a) SAMs originally formed on the Hg surface. (b) The molecules are packed more orderly. (c) Formation of Hg|H-Si≡ junctions at the defects (bare spots) after rearrangement of the alkanethiols behaving as resistors 43

Figure 3.16 XPS scan of a Si substrate modified with HC≡C-CH_2-NH_2 (a) and of a C60-functionalized silicon substrate (b). 45

Figure 3.17 High-resolution XPS scans showing the C1s and N1s regions. (a) and (b) are C1s peaks of HC≡C-CH_2-NH_2 modified Si substrate and of a C60-functionalized silicon substrate. (c) and (d) are N1s peaks of HC≡C-CH_2-NH_2 modified Si substrate and a C60-functionalized silicon substrate. 46

Figure 3.18 Current density-voltage (*J-V*) curves of HC≡C-CH_2-NH_2 SAM-modified silicon surface (a) and C60-functionalized silicon surface (b) with a Hg drop as the top contact electrode 47

List of Acronyms

µCP	Microcontact printing
A	Surface area
A*	Richardson Constant
CnSH	Alkanethiol
CNT	Carbon nanotube
d	Diameter
E_C	Conduction band
E_F	Fermi level
E_V	Valence band
$f_F(E)$	Fermi-Dirac distribution function
H-Si≡	Hydrogen-terminated silicon
J	Current density
J-V	Current-density versus voltage measurement
k	Boltzmann constant
MS	Metal-semiconductor
NW	Nanowire
ϕ	Work function
ϕ_{Bn}	Schottky barrier height
ϕ_{eff}	Effective barrier height
ϕ_M	Work function of metal
ϕ_n	Energy difference between E_C and E_F
ϕ_S	Work function of semiconductor
q	Elementary charge
R	Rectification ratio
SAM	Self-assembled monolayer
SiR_nX_{4-n}	Organosilanes
T	Absolute temperature
V	Voltage
V_{bi}	Built-in potential
V_F	Forward bias
V_R	Reverse bias

XPS	X-ray photoelectron spectroscopy
η	Ideality factor
X_S	Electron affinity of semiconductor

1. Introduction

The rapid development of large-scale integrated circuits has made modern electronic devices easier to build and to modify. The effect of scaling-down the dimensions of a semiconductor device has attracted tremendous attention from all over the world, as it eventually will result in more portable and lighter devices. Substantial efforts have been made on developing new fabrication methods or materials required to construct newer and smaller electronic devices. Nanoscience approach is one of the most popular choices, e.g., using carbon nanotubes (CNTs) and nanowires (NWs) for electronic devices.[1-3] These 1D structures can be used as building blocks for nanodevices, and attaching electric contacts (such as metal) to an individual nano-device is a first step towards integration.

Nowadays, scientists are also examing 2D nanostructures such as monolayers, particularly their effects on metal-semiconductor (MS) junctions. Here, metals serve as a necessary component to connect the semiconductors to the “outside world”. They may work as interconnects and provide the pathways to pass electrical signals to and from a device. Under proper conditions, they are also able to produce rectifying junctions that can be used to control the response of semiconductors by allowing current flow in only one direction, or ohmic contacts that allow electrons or holes to enter and leave the semiconductors with little resistivity. MS junctions have long been used in integrated circuits such as gate electrodes in typical metal semiconductor field effect transistors.[4] The electrical properties of a MS junction can be tuned by assembling organic monolayers on semiconductor surfaces.[5] These monolayers are certainly an appealing system for us to study as they may help us to achieve the goal of constructing molecular electronics (i.e., to use individual molecules as component elements in an integrated circuit).[6] However, the development of practical molecular electronic devices for the market is still in its infancy, with many fundamental questions remaining. The electrical properties of such metal-monolayer-semiconductor junctions, particularly the charge transport mechanism across the interface, are of practical importance. The aim

of this thesis is to investigate the effect of different monolayers embedded in metal-monolayer-semiconductor junctions on the observed electrical properties.

1.1. Metal-Semiconductor (MS) Junctions

1.1.1. History and Applications

The MS junction is also known as Schottky diode after Walter Schottky (1886-1976), a renowned German physicist. In fact, MS junctions were first reported by Karl Ferdinand Braun in 1874,[7] who studied the electrical properties of metallic contacts on copper, iron or lead sulfide crystals and found that the total resistance of the device varied with the direction of the applied voltage and surface conditions. By sharpening a metallic wire in contact with an exposed semiconductor, the rectifying behaviour could be enhanced, resulting in the point-contact diode. Point-contact diodes were used as radio wave detectors,[8] frequency converters and low-level microwave detectors in the early days of wireless technology.[9] Numerous experimental and theoretical studies of MS contacts have been carried out since the early 20th century, driven by the above mentioned applications.[10]

1.1.2. Electrical Properties of MS Junctions

Our understanding of the rectifying behavior of MS junctions was based on the contributions of Schottky who postulated a potential barrier at the metal-semiconductor interface.[11] The mechanism of barrier formation and models of calculating the barrier height were explained by Schottky[12] and Mott[13] in their subsequent seminal work. Here I will only give a brief introduction to the electrical properties of MS junctions.

The electrical properties of MS junctions depend on the type of metal and semiconductor incorporated. As silicon is one of the most frequently used semiconductor materials in electronic devices, it is chosen as the example to show how the potential barrier is formed at a MS interface. This potential barrier is responsible for controlling the direction of the current conduction as a result of work function differences between the metal and the semiconductor. The work function (ϕ) is defined as the energy required to remove an electron from the Fermi level (E_F) to vacuum. It is the minimum energy

required to remove an electron from the surface of material. The Fermi energy level is defined as the highest energy state at which electrons are occupied at 0 K, where all states below E_F are filled with electrons and all states above E_F are empty. If the temperature is above absolute zero, electrons can be excited by the thermal motions of the atoms and jump to higher energy levels, resulting in a change in the distribution of electrons among the available energy states. This can be calculated by the Fermi-Dirac distribution function (f_F(E)):[14-15]

$$f_F(E) = \frac{1}{1 + \exp(\frac{E - E_F}{kT})} \tag{1.1}$$

The function f_F(E) takes into account the effects of the particles being indistinguishable (i.e. they are identical) and the Pauli exclusion principle (no two electrons may occupy the same quantum state). It gives the probability that a quantum state at the energy E will be occupied by an electron. Under this condition, E_F is the probability of 0.5 of a state being occupied. In a metal, E_F is in an allowed half-filled highest occupied band in which there are many electrons available for conduction, leading to a high conductivity. In an intrinsic semiconductor, E_F is located at half of the band gap of the semiconductor and for an n-type semiconductor, E_F is closer to the conduction band than to the valence band. The conduction band (E_c) is the energy level in which electrons are mobile and thereby carry an electric current. The valence band (E_v) is usually located below the E_c of a semiconductor, which is the range of energy states that filled with electrons at absolute zero temperature. The electron affinity of a semiconductor ($q\chi_S$) is the energy difference between the bottom of the conduction band and the vacuum level. In Figure 1.1, the metal's work function ($q\phi_M$) is assumed to be larger than the semiconductor's work function ($q\phi_S$). Therefore, before contact (Figure 1.1 (a)), the Fermi level in the semiconductor is above that in the metal. When the metal and the semiconductor are brought into contact with each other, their Fermi levels need to align themselves through the systems in thermal equilibrium. Electrons will flow from the conduction band of the semiconductor into the lower energy states in the metal, leaving some region (named as depletion region) in the semiconductor positively charged. The formation of the depletion region will lead to the bending of the

semiconductor bands, resulting in a barrier ($q\phi_{Bn}$) seen by electrons in the metal trying to move into the semiconductor.

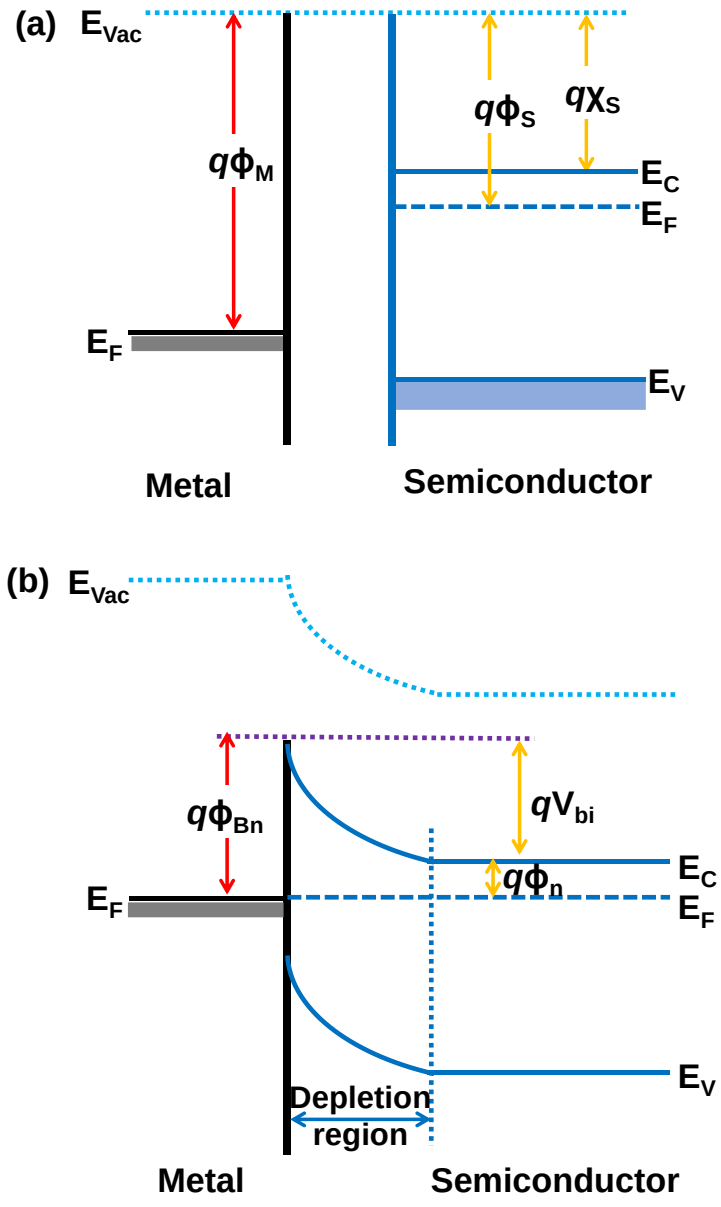

Figure 1.1 Energy-band diagram of a metal and semiconductor (a) before contact and (b) after contact. E_F is the Fermi level and E_C and E_V are the conduction band and the valence band of the semiconductor. $q\phi_M$, $q\phi_S$, $q\chi_S$ and $q\phi_n$ are the metal work function, the semiconductor work function, the electron affinity of the semiconductor and the energy difference between E_C and E_F, respectively.

For ideal Schottky junctions, the barrier height $q\phi_{Bn}$ is the energy difference between the metal work function and the semiconductor's electron affinity if the image-lowering effect and surface states are not considered. The barrier $q\phi_{Bn}$ is also known as the Schottky barrier:

$$q\phi_{Bn} = q\phi_M - q\chi_S \tag{1.2}$$

where q is the elementary charge. V_{bi} is the built-in potential barrier on the semiconductor side which is seen by electrons moving from the conduction band of the semiconductor into the metal:

$$qV_{bi} = q\phi_M - q\phi_S \tag{1.3}$$

If a positive voltage is applied to the metal with respect to the semiconductor, which is the forward bias condition, electrons will transfer more easily from the semiconductor into the metal as the barrier on the semiconductor side is reduced by the applied voltage (V_F) (Figure 1.2 (a)). On the other hand, for a reverse bias condition a positive voltage is applied to the semiconductor and the Schottky barrier $q\phi_{Bn}$ will not be influenced by the reverse bias (V_R). Therefore, electrons moving from the metal to the semiconductor will overcome the same barrier height as the metal-semiconductor after contact (Figure 1.2 (b)).

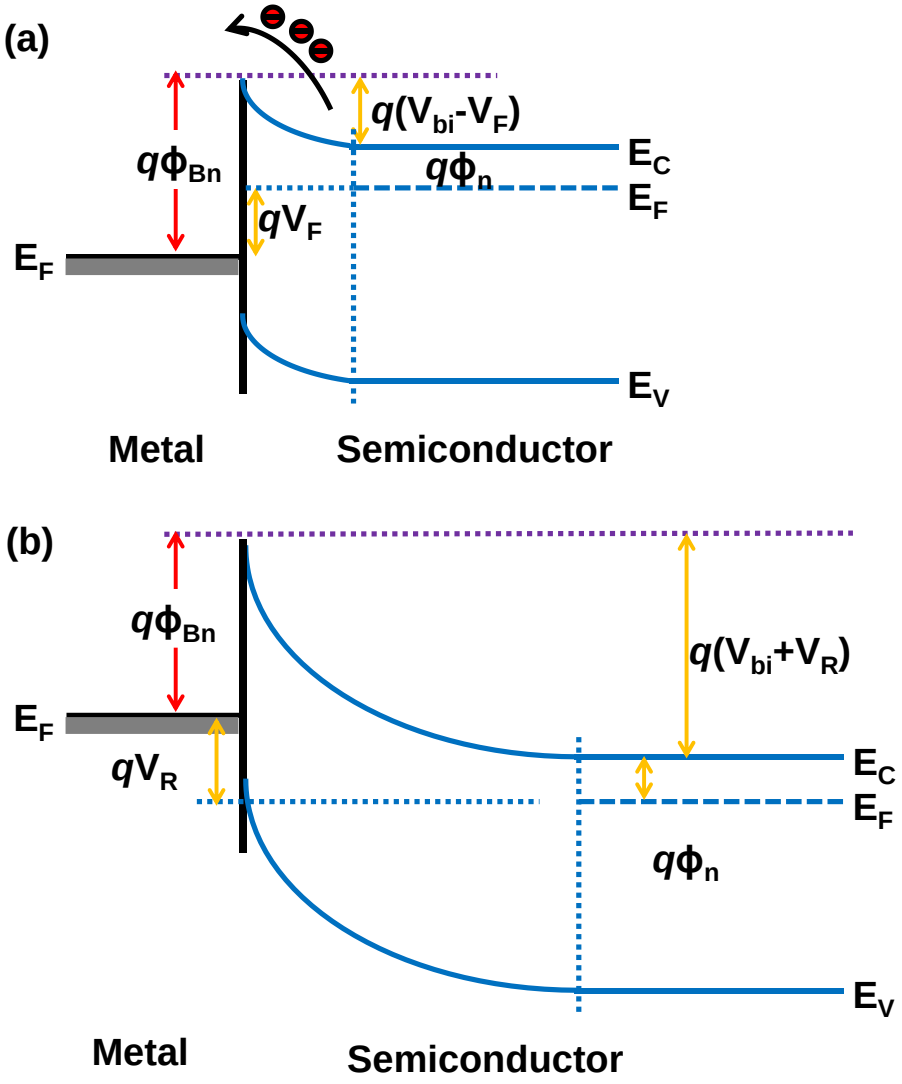

Figure 1.2 Energy-band diagram of a MS junction under (a) forward bias and (b) reverse bias. V_F is the magnitude of the forward bias while V_R is the magnitude of the reverse bias.

The current transport mechanism for a MS rectifying junction is due mainly to the flow of majority carrier electrons over the potential barrier which can be explained by the thermionic emission theory. If we assume that the barrier height is much larger than *kT* and thermal equilibrium is not affected, the total current density (*J*) given by the thermionic theory is as follows:

$$J = J_{S \to M} - J_{M \to S} \tag{1.4}$$

where $J_{S\rightarrow M}$ is the current density from semiconductor to metal for the concentration of electrons with energies sufficiently high to jump over the barrier while $J_{M\rightarrow S}$ is for electrons moving from the metal into the semiconductor. $J_{S\rightarrow M}$ can be written as

$$J_{S\rightarrow M} = A^{*}T^{2}\exp\left(\frac{-q\phi_{Bn}}{kT}\right)\exp\left(\frac{qV}{kT}\right) \tag{1.5}$$

where A^{*} is the Richardson constant of the thermionic emission theory, V is the applied voltage, k and T are Boltzmann's constant (1.38×10^{-23} $m^2kgs^{-2}k^{-1}$) and absolute temperature. For ideal Schottky junctions, the barrier height $q\phi_{Bn}$ is the energy difference between the metal work function and the semiconductor's electron affinity if the image-lowering effect is not considered.

Since the barrier height for electrons moving from metal into semiconductor remains the same under both forward bias and reverse bias, the current transport in the junction will not be affected by the applied voltage. It is equal to the current at the condition of thermal equilibrium, i.e., $V = 0$,[14-15]

$$J_{M\rightarrow S} = -A^{*}T^{2}\exp\left(\frac{-q\phi_{Bn}}{kT}\right) \tag{1.6}$$

Then, J is given by

$$J = \left[A^{*}T^{2}\exp\left(\frac{-q\phi_{Bn}}{kT}\right)\right]\left[\exp\left(\frac{qV}{kT}\right) - 1\right] \tag{1.7}$$

1.2. Self-Assembled Monolayers (SAMs)

The properties of a solid surface may be conveniently modified with self-assembled monolayers (SAMs). These SAMs are formed spontaneously upon immersion of a solid substrate into a dilute solution of molecules which have high affinity

toward the surface.[16] Early work included the use of alkyl trichlorosilanes which is moisture-sensitive on hydrophilic glass. This was followed by applying alkanethiols on crystalline gold surfaces. The organization and properties of these SAMs have been investigated by means of spectroscopy, microscopy, electrochemistry and many other surface techniques.[17-19] SAMs are well used in nanoscience and technology because they have a number of special properties. They are a particular form of nanoscale organic films because the thickness of SAMs is usually 1-3 nm. They can be fabricated into nanoscale dimension patterns via soft lithography,[20] or by microcontact printing (μCP).[21]

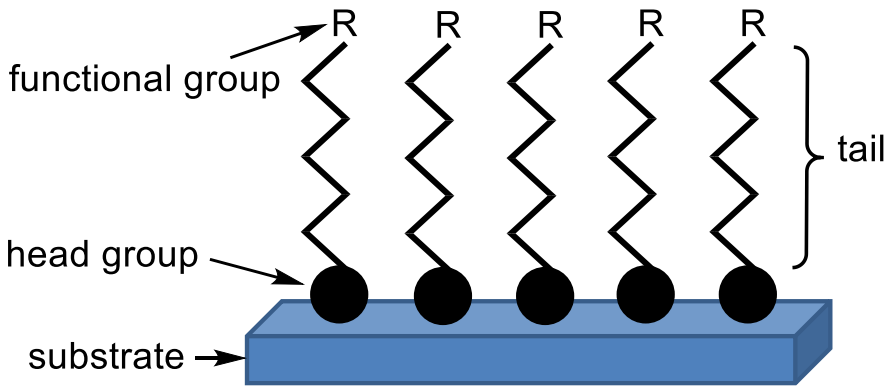

Figure 1.3 Idealized representation of a self-assembled monolayer (SAM) on a solid substrate.

SAM-forming molecules usually have (i) one head group that has a high affinity to the substrate, (ii) alkyl chains or aromatic rings that play a crucial role in the ordering or packing of the monolayer on the substrate, and (iii) a functional group which introduces another possibility for interacting with the environment (Figure 1.3).The head group initiates the most important exothermic process by chemisorption to the substrate surface. This results in its apparent pinning to a specific site on the surface through a chemical bond. As a result of the exothermic head group-substrate interactions, molecules try to occupy all available binding sites on the surface, and in this process they push together molecules that have already adsorbed. These adsorbates organize into ordered and closely packed crystalline (or semicrystalline) structures. Short-range Van der Waals forces (in case of simple alkyl chains) or long-range electrostatic interactions (in case of a polar bulky group) are the main forces that bring molecules together.

Among different kinds of SAMs, alkanethiolate monolayers on gold have been studied most thoroughly. Alkanethiols (CnSH) have a strong affinity to Au surfaces[22] and chemisorb spontaneously on a gold surface. The energy associated with this chemisorption is in the order of hundreds of kJ/mol (~128 kJ/mol[23]). SAMs of alkanethiols with n > 11 on gold surfaces form well-ordered, close-packed monolayers.[24-26] The most widely used process for preparing SAMS on gold is immersion of a gold substrate in a freshly prepared dilute (1-10 mM) ethanol solution of thiols for about 12-18 h at room temperature.[27] The formation of alkanethiolates on gold is a relatively fast process (milliseconds to minutes). These adsorbates will undergo a slow reorganization process which takes a few hours in order to generate a high density of molecules on the surface and reduce the defects in the SAM.[27-28] In practice, the acquisition of low-defect density SAMs is quite important because their desired functional behaviors such as wettability, corrosion and charge-transfer processes are heavily influenced by the defects. Therefore, the experimental factors (immersion time, concentration of adsorbate, solvent and temperature) that can affect the structure need to be optimized. Ethanol is the most commonly used solvent for preparing alkanethiolate SAMs on gold surfaces[27] as most alkanethiols are soluble in ethanol. In addition, it is available in high purity, with low price and low toxicity. The kinetics of SAM formation can be improved by raising the temperature. The chemisorption and reorganization of SAM happens in the first few minutes of the formation, which depends on the temperature.[29] The concentration of thiols and immersion time are inversely related, i.e., high concentrations of thiols in solution require short immersion time.[30]

Besides alkanethiols on gold, the self-assembly of organosilane molecules on hydroxylated surfaces has also been well studied. An organosilane is a molecule consisting of one Si atom connected with four functional groups, SiR_nX_{4-n}, where $–R_n$ is the organic functional group and $–X_{4-n}$ is the head group. The head groups are hydrolysable, (such as methoxy, ethoxy and chloride) and react with hydroxyl groups on an oxide surface. The preparation of a monolayer of silanes on a surface needs a trace amount of water. Halogen or alkoxy groups in an organosilane molecule are converted to hydroxyl (–OH) groups by hydrolysis. The silanols (Si–OH) react with –OH groups on the surface of an oxidized Si substrate, thereby immobilizing the molecules on the surface through siloxane (Si–O–Si) bonds. Organic monolayers with low surface energy

on inorganic materials have been prepared by this surface modification chemistry,[31] which is known as silane-coupling.[32]

1.2.1. SAMs on Hg

For solid-supported alkanethiolate SAMs, the strong interactions between thiols and gold lead often to an order-induced epitaxiality by the crystalline structure of the substrate. The strong chemisorption of the thiol head group makes these SAMs robust which is a very desirable quality for the application of devices. However, it has been found that alkanethiolate SAMs on solid surfaces have pinholes and other defects,[33] which prevent applications that require complete blocking of charge transport. This is because solid surfaces cannot be atomically flat over large areas. Therefore, mercury, as a liquid metal, which has a homogeneous, reproducible atomically flat and defect-free surface and electronic conductivity is an ideal surface for preparing pinhole-free SAMs.

Alkanethiols have strong affinity toward Hg, too. The packing of their SAMs is controlled by interactions between adsorbed molecules,[34] rather than by the crystal lattice surface.[19] The Weaver group found monolayers formed from short-chain, cyclic thiols on Hg are more impermeable than those formed on Au surfaces due to the fluidity of the Hg surface.[35] Clearly, defect-free films would be desirable for characterizing the intrinsic properties of the films, and many other applications, like electron-transfer studies, could also benefit. The first research to address the characterization of extremely low defect-density long-chain alkanethiolate SAMs on Hg was done by Harrison and co-workers.[35] They measured the electrochemical impedance spectroscopy (EIS) for both bare and hexadecanethiol (C16SH)-modified Hg drops in electrolyte solutions free of electroactive species, and concluded that C16SH formed an impermeable, pinhole-free layer on Hg.[36] Images of octanethiol (C8SH) SAMs on Hg drops were obtained by using scanning tunneling microscopy (STM).[37] The properties, structure and the macroscopic phase transitions of these SAMs upon compression/expansion of the Hg drop were examined by the Caldwell group.[38] They found that it is possible to control the packing of alkanethiols by changing the size of the Hg drop, and the permeability of the SAMs was dependent on the alkanethiol chain length.[38] Later, the Majda group investigated the influence of the monolayer thickness and found that alkanethiols with chain lengths from C9SH to C14SH are able to form

densely packed, perpendicularly oriented monolayers on a hanging mercury electrode.[39-40] They proposed two pathways for electron tunneling caused by through-bond and chain-to-chain coupling.[39, 41] The White group investigated the oxidative adsorption of alkanethiolates from a Hg surface in basic aqueous solutions by means of cyclic voltammetry. They showed that a critical value of the alkyl chain length sets the limit for the formation of densely packed monolayers, and that the formation of alkanethiolate SAMs on Hg is energetically favorable and potential-dependent.[42] The Mandler group found that an organized aggregation of alkanethiols leads to a condensed film after adsorbing on the Hg surface; two states exist for alkanethiolate adsorption on Hg as evidenced by their voltammetry and differential capacitance measurements.[43-44] The coverage-dependent phase behavior of these monolayers has been studied by Ocko and Deutsch. They concluded that at low coverage, a surface-parallel monolayer was formed, but at high coverage a monolayer of standing-up molecules was generated.[45-46]

The electrochemistry of alkanethiolate SAMs on Hg in aqueous solutions has been intensively investigated. It is generally accepted that the adsorption of alkanethiols on metallic Hg can be described by an oxidation process that is similar to the self-assembly process on gold surfaces

$$\alpha \mathrm{Cn}SH + Hg \rightarrow Hg(SCn)_{\alpha(ads)} + \alpha H^{+} + \alpha e^{-} \qquad \alpha = 1 \; or \; 2 \tag{1.8}$$

The fast irreversible adsorption of thiols on Hg results in mercurous- or mercuric-thiolate adducts.[47-48] The final oxidation state of the mercury is still unclear. Recent electrochemical studies and elemental analysis of the bulk synthesis products of alkanethiols in aqueous media[49] and organic solvents[39] showed that the formation of mercuric thiolates and alkanethiol self-assembly are associated with a transfer of one electron per thiol. The Majda group revealed that the atomic ratio of Hg:S is 1:2 indicating that mercuric alkanethiolates are formed.[39]

1.2.2. SAMs on Si

Organosilane molecules have been shown to readily self-assemble as monolayers on different kinds of hydroxylated surfaces, like SiO_2 on Si substrates in the

presence of a residue of water.[50] However, the organosilane SAMs have a disadvantage from the viewpoint of electronic applications. The formation of such SAMs requires the presence of a thin 1-2 nm thick oxide layer which interferes the electrical properties of the Si substrates. Besides, these monolayers are not uniform and not stable enough for extensive chemical studies or effective isolation of the underlying substrate for electrical measurements. Therefore, it is important to find a method to modify the oxide-free Si surface by introducing a strong chemical bond. The formation of covalently bonded organic monolayers on the hydrogen-terminated Si surface (H-Si≡) is an effective way to generate a passivation layer.[51] Alkyl monolayers may be formed on silicon by UV exposure,[52] thermal reaction,[53] or Grignard reaction.[54] Furthermore, 1-alkynes are more reactive than 1-alkenes on H-Si≡.[55] The surface coverage was measured to be approximately 50%[53] for alkyl monolayers and close to 65% for alkenyl monolayers.[56]

The proposed mechanism for this type of reaction, using diacyl peroxides ($[CH_3(CH_2)_nCOO]_2$, n = 16 or 10) as example, is as follows: First, the diacyl peroxide undergoes homolytic cleavage to form two alkoxy radicals ($[RCOO]_2 \rightarrow 2\ RCOO\cdot$). This is followed by the generation of alkyl radicals via decarboxylation ($RCOO\cdot \rightarrow R\cdot + CO_2$). Then a silicon radical is formed from H-Si≡ and an alkyl radical by hydrogen abstraction by the alkyl radical ($R\cdot + H\text{-}Si \rightarrow H\text{-}R + Si\cdot$). Finally an alkyl radical combines with silicon to form the monolayer ($R\cdot + Si\cdot \rightarrow Si\text{-}R$).

The mechanism of thermal reaction (Figure 1.4) is similar to the diacyl peroxide-promoted reaction. The silicon radical is formed by extracting a hydrogen from the silicon surface by heating it to a temperature above 150 ˚C. Then a terminal alkene or alkyne reacts with the silicon radical to create a covalent bond, resulting in another radical on the second carbon in the chain. This newly formed radical on a methylene (CH_2) group can then subtract a hydrogen atom from an adjacent H-Si to continue the reaction.[51] It is also possible to form a monolayer on top of H-Si without UV exposure or thermal heating at room temperature at a slow reaction rate.[57]

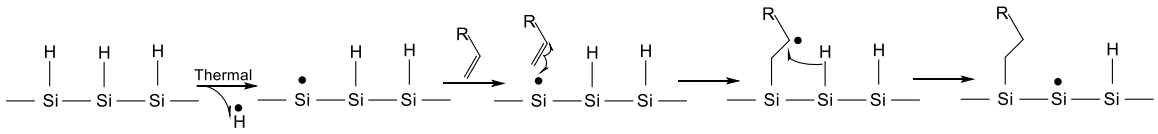

Figure 1.4 Mechanism of terminal alkene reaction with H-Si≡ via radical initiation.

1.3. Metal-Monolayer-Semiconductor Junctions

The incorporation of a monolayer of the MS junction creates a metal-monolayer-semiconductor junction and provides the capability to modify its electrical characteristics at the nanoscale.[58] Typically, the formation of metal contacts on organic monolayers is a destructive process, as high-energy metal atoms from most deposition techniques such as thermal evaporation or sputtering will damage or even displace the organic molecules.[59] Furthermore, gold, as a metal contact, will react with remaining H-Si≡ at a monolayer-silicon surface to form an Au-Si alloy. Therefore, mercury, as a liquid metal, is chosen as the contact in MS junctions. Due to its high surface tension and low reactivity, it will not "short" an MS junction by passing through the monolayer.[60-61]

1.3.1. Hg | Monolayer-Si≡ (R-Si≡) Junctions

The application of a mercury drop (Hg) as the top metal contact for preparing metal-monolayer-semiconductor junctions has been explored previously to study a diverse set of monolayers, particularly their effects on the electrical performance of the modified junctions. By modification with an alkyl monolayer, we were able to tune a Hg|H-Si≡ junction which behaved as a resistor to a Hg|monolayer-Si≡ junction which behaved as a diode (Figure 1.5).[62]

These monolayers were found to be robust and uniform, suitable for current-voltage and capacitance-voltage measurements. Their stability suffers from a slow oxidation process which also affected their electrical performance.[63] Investigations of the charge transport through such a metal-monolayer-semiconductor junction led to the conclusion that chemical bonding was not an important factor for tunneling through alkyl chains.[60, 64-65]

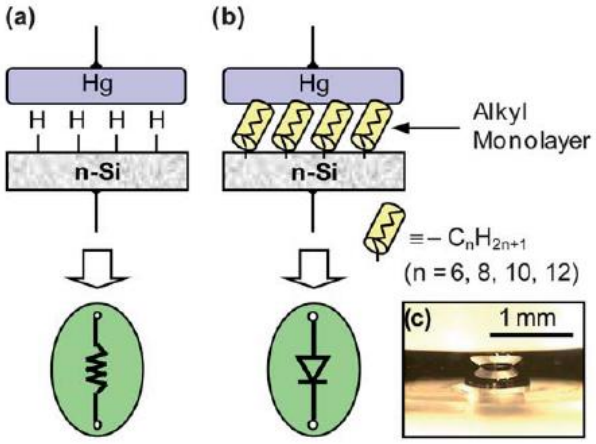

Figure 1.5 Schematic illustration of the electrical properties of a Hg|H-Si≡ junction vs. a Hg|monolayer-Si≡ junction.

1.3.2. Hg-Monolayer|H-Si≡ Junctions

Alkanethiolate SAMs on Hg have been studied in solution via electrochemical measurements as mentioned above. It is of practical importance to study Hg-monolayer|H-Si≡ junctions because most electronic devices are used in the solid state. Furthermore, these solid state measurements permit the investigation of electron transport through the interfacial alkyl monolayers without the interference of solution diffusion.[65] This type of junction has not yet been studied extensively but several researchers did examine Hg-SAM||SAM-metal junctions in the past. The Whitesides group studied Hg-SAM||SAM-Hg junctions in basic aqueous solutions of $Ru(NH_3)_6Cl_3$ which are redox centers that can transport charge between the electrodes.[66] They found that the electrical characteristics of these junctions were initially determined by a redox-cycling mechanism when the electrode separation was minimal, and changed to a conduction mechanism dominated by the physical diffusion of $Ru(NH_3)_6^{3+/2+}$ to the electrode surface after repeated measurements, with a contribution of electron hopping to charge transport.[66] These authors also created and examined Hg-SAM||SAM-Ag junctions, for which current rectification was observed.[61]

1.4. Objectives of This Thesis

Previous studies have shown that for monolayers covalently bonded to an oxide-free silicon surface, direct thermal metal (usually gold) deposition typically causes a disruption in the ordering of the monolayer. Therefore, a mercury drop (as a soft contact) has been used to examine metal|monolayer|silicon junctions. Assembling an organic monolayer on a Si substrate is the most commonly used method to tune the electrical property of a MS junction. Little research has been done on assembling a monolayer on the metal side. The objective of my research was to construct Hg-SAM|H-Si≡ junctions and carry out solid-state electrical characterization of such junctions. This research can be considered significant as electronic devices are typically solid-state, as opposed to solution phase.

My project initially focused on using an octadecanethiolate (C18) SAM on Hg for preparing Hg-S-C18|H-Si≡ junctions. Octadecanethiol was chosen because it has been shown to form a densely packed monolayer on a Hg surface. Electrical measurements were the key characterization method used to study the system: conventional current density-voltage (*J*-*V*) properties were examined by manual manipulation of the size and shape of the Hg drop. Electron transport properties across the molecular junctions were studied, and the *J*-*V* curve was analyzed using the thermionic emission model. Rectification ratios, ideality factors and barrier heights were calculated to better understand the system. Subsequently, molecular junctions formed with SAMs of various alkyl chain lengths on the Hg electrode were studied. The modification of silicon was not limited to small molecules like alkanethiolates; larger molecules such as fullerenes (C60 was used here) can also be immobilized on the silicon, between the mercury and silicon interface, to form nanostructures. These nanostructures could be studied by scanning tunneling microscope (STM) after gold deposition. I, therefore, also initiated a project to study the effect of these nanostructures on MS junctions, i.e., the preparation and preliminary characterization of Hg|C60-Si junctions.

2. Experimental Section

2.1. Materials and Reagents

1-decanethiol (C10SH, 96%), 1-undecanethiol (C11SH, 98%), 1-dodecanethiol (C12SH, 98%), 1-tetradecanethiol (C14SH, 94%), 1-hexadecanethiol (C16SH, 97%), 1-octadecanethiol (C18SH, 98%), propargylamine ($HC{\equiv}C\text{-}CH_2\text{-}NH_2$,98%), fullerene ($C_{60}$, 99.5%), hexaammineruthenium (III) chloride ($Ru(NH_3)_6Cl_3$, 98%), tetrahydrofuran (THF), trifluoroacetic acid (TFA), and dichloromethane were purchased from Sigma-Aldrich. These chemicals were of ACS reagent grade and used without further purification. Sulphuric acid (H_2SO_4, 96%), hydrogen peroxide (H_2O_2, 30%), and ammonium fluoride (NH_4F, 40%) were complementary metal-oxide-semiconductor grade and purchased from Anachemia Science. Decane (anhydrous, ≥ 99%) was bought from Sigma-Aldrich and distilled once in the presence of sodium to get rid of the impurities.

Mercury was washed with 1 M HNO_3 and filtered through a folded filter paper (with a small hole at the bottom). Silicon wafers (n-type Si (111), phosphorus-doped, 0.5-5 Ohm·cm, single-sided polished) were purchased from Virginia semiconductor, Inc.

2.2. Sample Preparation

2.2.1. Preparation of Hydrogen-terminated Silicon (H-Si≡)

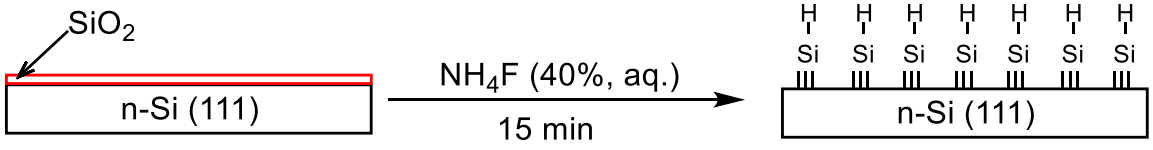

Figure 2.1 Schematic illustration of the preparation of H-Si≡.

Si (111) wafers were first cut into small pieces (1.0 cm × 2.5 cm) and cleaned by sonication in ethanol (95%) for 10 min. The samples were then rinsed with deionized water (18.3 MΩ·cm) and submerged in a “piranha solution” at 90 °C for 30 min. Piranha solution is a 3:1(v:v) solution of 96% H_2SO_4 and 30% H_2O_2. *Caution: “Piranha solution” is highly reactive and should be handled with extreme care.* This was followed by thorough washing with deionized water. Finally, the silicon wafers were etched for 15 min with NH_4F (40%) which was deoxygenated by Ar gas for 30 min to remove the native oxide layer. The wafers were washed by a trace amount of water to obtain hydrogen-terminated silicon (H-Si≡).

2.2.2. Preparation of a Hg-SAM|H-Si≡ Junction

A Hg-SAM|H-Si junction was formed using a custom-built device as depicted in Fig. 2.2. A 1.0 mL gas-tight syringe filled with mercury was fixed on a vertically movable stage and positioned vertically. A small glass cell was placed below the syringe allowing for immersion of the hanging mercury drop (extruded from the syringe) in a desired alkanethiol solution or pure solvent. A self-assembled monolayer of alkanethiols on mercury was formed by immersing the Hg drop in a ~5 mM solution of $CH_3(CH_2)_{n-1}SH$ (n = 10, 11, 12, 14, 16, 18) in ethanol (95%) for 10 min. Subsequently the Hg drop was cleaned twice with ethanol (95%) and once with water and dried in air. The modified Hg drop was then used to form Hg-S-Cn|H-Si≡ junctions, upon carefully lowering the syringe. The syringe was lowered slowly to avoid any disturbance to the Hg drop. The Hg drops with low quality SAMs, i.e. the formed junctions behaved as resistors or the current density under reverse bias was almost at the same level of that under forward bias, would be abandoned.

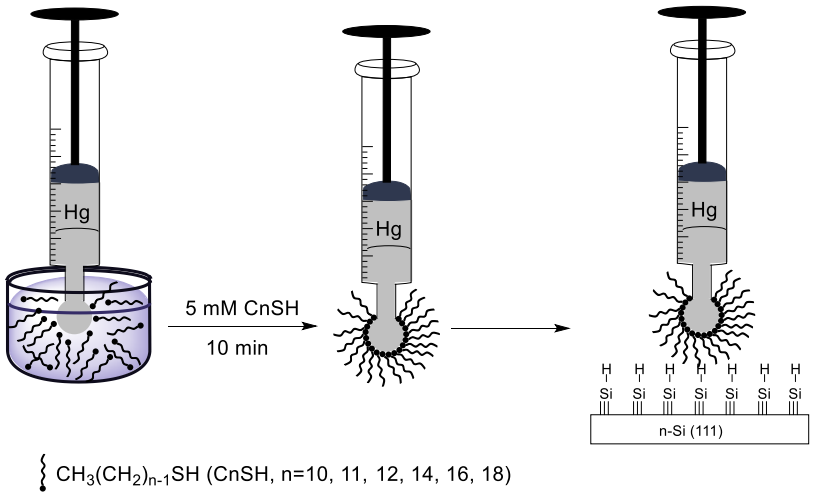

Figure 2.2 Schematic view of the formation of a Hg-S-Cn|H-Si≡ junction.

2.2.3. Formation of a Hg|R-Si≡ Junction

A freshly prepared H-Si≡ wafer was put in a Schlenk tube containing a 500-mM C12SH solution in decane and heated in a silicone oil bath at 150˚C for 5 hours under Ar atmosphere. The monolayer-modified Si was cleaned at room temperature with 2% TFA in THF, by sonication in dichloromethane for 30 s and then dried by a stream of N_2. Similar to the procedure shown above, a bare Hg drop was used to fabricate the Hg|C12-S-Si≡ junctions.

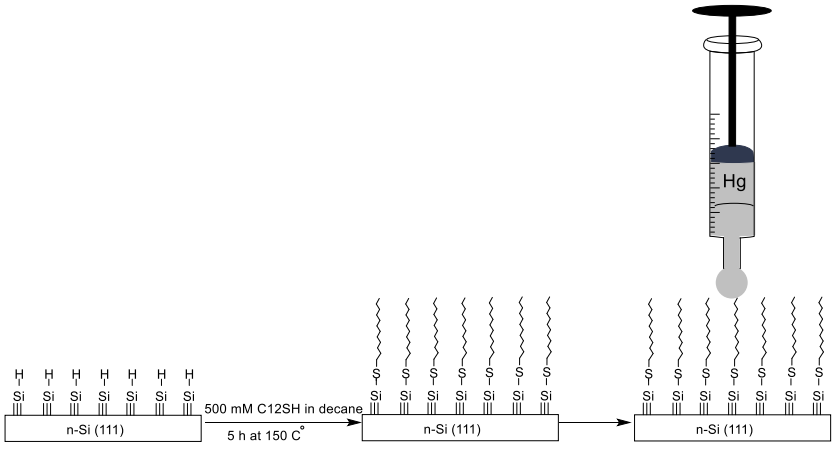

Figure 2.3 Formation of a Hg|R-Si≡ junction. The monolayer-modified Si was cleaned with 2% TFA in THF, sonication in dichloromethane for 30 s and then dried by a stream of N_2.

2.3. Solid-State Electrical Measurements

Current density versus voltage (*J*-*V*) measurements were carried out using the setup shown in Figure 2.4. The backside of the silicon wafer was scratched with a diamond knife for depositing the InGa eutectic paste that was essential for establishing an ohmic contact. Then the sample was placed on top of a copper block for making the Hg-SAM|H-Si≡ (Figure 2.4 (a)) or Hg|R-Si≡ junctions (Figure 2.4 (b)). The measurements were carried out in a Faraday cage. The junction contact area was determined by using a digital video microscope (40× objective lens) upon forming the junction. The microscope was calibrated with a standard circle which had a diameter of 1000±50 µm. Therefore, we estimated a ±5% precision of the contact diameter determination. An Autolab electrochemical analyzer (PGSTAT30, Eco Chemie BV, The Netherlands) carried out the electrical measurements. The current-voltage (*I*-*V*) curves were typically taken between – 1.0 V and + 1.0 V range. At forwards bias scans (V>0), the Hg was positive with respect to the n-type silicon.

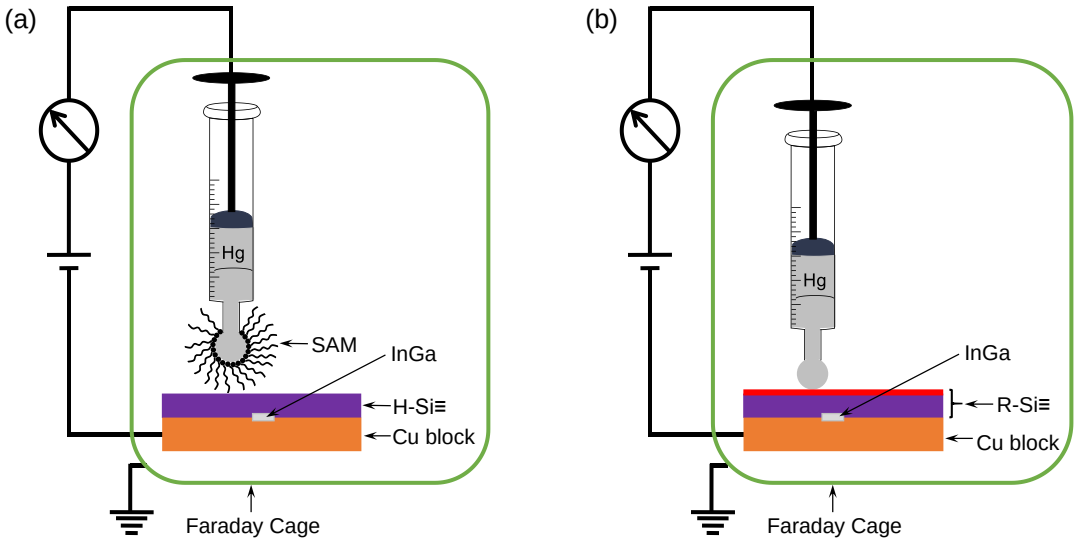

Figure 2.4 Schematic view of the apparatus used to measure current density versus voltage properties: (a) a Hg-SAM|H-Si≡ junction; (b) a Hg|R-Si≡ junction.

2.4. Electrochemical Studies of SAMs on Hg

Electrochemical measurements were performed in a conventional three-electrode glass cell. The working electrode was the mercury drop controlled by the gas-tight syringe as mentioned above. After the Hg drop was modified with a C18SH SAM, the syringe was transferred to the electrolyte solution. A platinum wire with a diameter of 0.025 mm was used as counter electrode and the distance from the working electrode was kept as 1.5 cm. An Ag|AgCl|3 M NaCl electrode was used as reference electrode, and the supporting electrolyte was 0.1 M KCl. 5.0 mM $Ru(NH_3)_6^{3+}$ was added to the electrolyte for the cyclic voltammetry measurements. These measurements were performed with an Autolab electrochemical analyzer (PGSTAT30, Eco Chemie BV, The Netherlands) in a Faraday cage. All data were collected at a scan rate of 50 mV/s at room temperature.

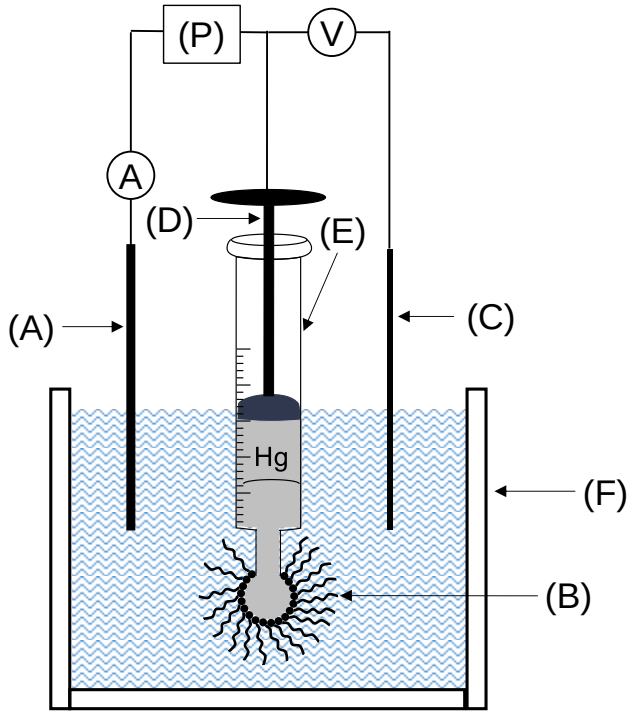

Figure 2.5 Electrochemical setup with the SAM modified Hg drop as the working electrode. (A) Ag|AgCl|3M NaCl reference electrode, (B) Hg drop modified with an alkanethiolate SAM, (C) platinum counter electrode, (D) tungsten wire connecting the Hg working electrode, (E) the gas-tight syringe, and (F) a glass cell of approximately 40 mL volume, (P) potentiostat.

2.5. Formation of Fullerene Monolayers on Si Surface

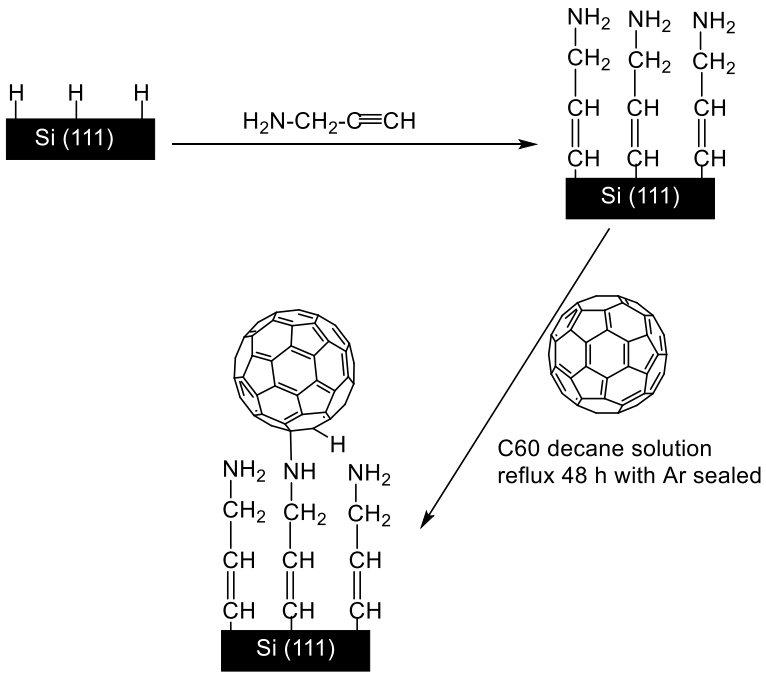

Figure 2.6 Immobilization of C_{60} on hydrogen-terminated Si surface.

The H-Si≡ sample was immersed in 150 mM propargylamine ($HC{\equiv}C\text{-}CH_2\text{-}NH_2$) solution in decane with Ar sealed, and heated to 90℃ for 4 h. The modified silicon wafer was cleaned with dichloromethane and 2% TFA in THF and then dried with N_2. Then the silicon wafer was transferred to 150 μM C_{60} solution in decane and refluxed for 48 h at 100˚C under Ar. The formation of C_{60} involved the reaction of the amine group with C=C bonds in C_{60}.[67] The same setup (Figure 2.4 (b)) was used to obtain preliminary results for the electrical properties of Hg|fullerene-Si≡ junctions.

3. Results and Discussion

3.1. Electrical Properties of Hg-S-C18|H-Si≡ Junctions

3.1.1. Volume Expansion of the Hg Contact

As mentioned in section 2, the octadecanethiolate (C18) SAM on Hg was prepared first, then the Hg drop was brought into contact with the silicon substrate, leading to the formation of Hg-S-C18|H-Si≡ junctions. The size of the Hg drop was increased gradually via ejecting additional Hg from the syringe.

The current density versus voltage (*J*-*V*) plots of the Hg-S-C18|H-Si≡ junction upon enlarging the volume of the mercury drop are shown in Figure 3.1(a). In comparison with the symmetric *J*-*V* curve observed for an Hg|H-Si≡ junction which behaves as a resistor (ohmic behavior),[62] the as-prepared Hg-S-C18|H-Si≡ junction shows the rectifying property of a diode, i.e., the current densities at forward bias are much higher than the saturation current at the reversed bias. The junction remained as a rectifying contact when increasing the size of the Hg drop initially, illustrated in Figure 3.1 (a) with green and blue lines. Further expansion of the mercury drop led to a remarkable change of the *J*-*V* properties from rectifying to ohmic (red curve in Figure 3.1 (a)). It is evident that the electrical property changes of the molecular junctions are directly affected by the “mechanical manipulation” of the mercury drop.

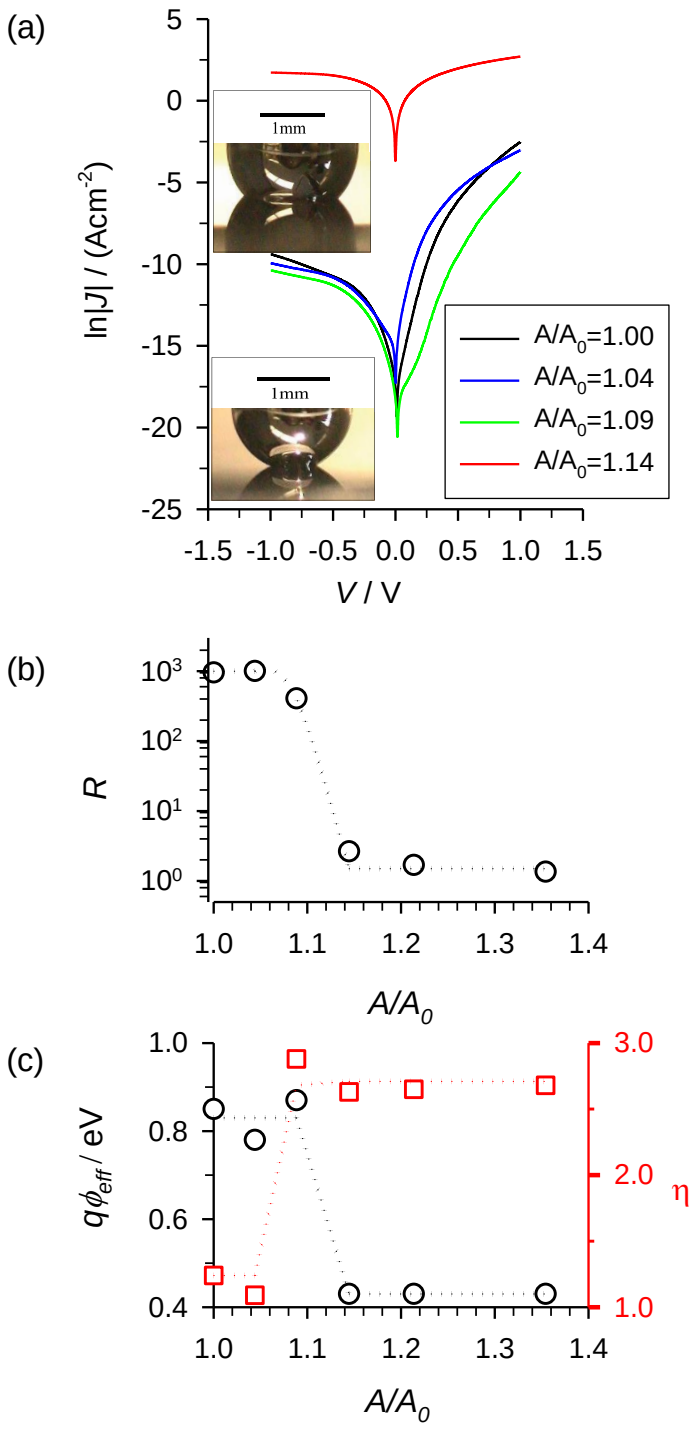

Figure 3.1 (a) Representative current-density vs. voltage (*J-V*) plots of a Hg-S-C18|H-Si≡ junction upon enlarging the Hg drop volume. (b) Rectification ratio (*R*) vs. surface area ratio, and (c) barrier height $q\phi_{eff}$ (black circles) and ideality factor η (red squares) vs. A/A_0.

The surface area (*A*) of a mercury drop at each volume was calculated from its shape. In Figure 3.2, we have shown the spherical shape of an as-prepared mercury drop. The surface area A_{sph} in this case can be calculated from equation 3.1,

$$A_{sph} = 4\pi\left(\frac{d_2}{2}\right)^2 - \pi\left(\frac{d_1}{2}\right)^2 \quad (3.1)$$

where d_1 and d_2 were determined from the optical image (40× magnification). The surface area (*A*) is compared to the original surface area A_0 (before any mechanical manipulation) to determine the ratio A/A_0 and calculate the percentage increase. The results derived from equation 3.1 are summarized in Table 1.

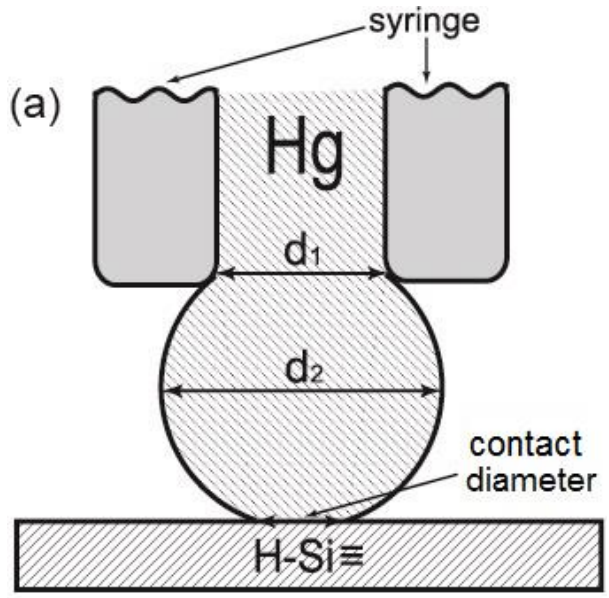

Figure 3.2 Schematic view of the spherical shape of a Hg drop upon forming contact with H-Si≡ as initially prepared and after volume expansion. (The schematic view is around 25 times larger than the real size of Hg drop.)

Table 3.1 Volume expansion of Hg drop

contact diameter (mm)	d_1 (mm)	d_2 (mm)	A_0 (mm^2)	A (×10 mm^2)	A/A_0
0.63±0.03	1.00±0.05	1.65±0.08	9.70±0.88		
0.71±0.04	1.00±0.05	1.74±0.09		1.01±0.09	1.04±0.14
0.85±0.04	1.00±0.05	1.77±0.09		1.06±0.10	1.09±0.14
1.05±0.05	1.00±0.05	1.85±0.09		1.11±0.10	1.14±0.15
1.21±0.06	1.00±0.05	1.92±0.10		1.18±0.11	1.21±0.16
1.44±0.07	1.00±0.05	2.05±1.10		1.31±0.12	1.35±0.18

The surface area ratio (A/A_0) allowed us to track the volume expansion process. We plotted the rectifying ratio (R), defined in equation 3.2, as function of surface area ratio (A/A_0) to illustrate the unique *J-V* switching property and to determine if at a specific threshold area ratio the *J-V* property of the Hg-S-C18|H-Si≡ junction suddenly changes.[68]

$$R = \left|\frac{J(+1.0\ V)}{J(-1.0\ V)}\right| \tag{3.2}$$

where J (+1.0 V) is the current density at +1.0 V and J (−1.0 V) is the current density at −1.0 V. As shown in Figure 3.1(b), the R value remained nearly unchanged at the level of 1000 with the surface area increasing by 4%. It dropped to around 400 at A/A_0 =1.09. Then a sudden decrease of the R value to around 1 was observed as the A/A_0 increased to 1.14. An R value of 1 means that the reverse current density is identical to that at forward bias, indicative of ohmic characteristics of the junction.

To further understand how electrical properties change upon enlarging the Hg drop, we applied classical thermionic emission theory to analyze the *J-V* curves, i.e., to determine the effective barrier height ($q\phi_{eff}$) and ideality factor (η) from the equations below,[14-15]

$$J = \left[A^* T^2 \exp\left(\frac{-q\phi_{eff}}{kT}\right)\right] \exp\left(\frac{qV}{\eta kT}\right)\left[1 - \exp\left(\frac{qV}{kT}\right)\right] \tag{3.3}$$

$$\ln\left[\frac{J}{1-\exp\left(-\frac{qV}{kT}\right)}\right] = \ln(A^*T^2) - \frac{q\phi_{eff}}{kT} + \frac{qV}{\eta kT} \tag{3.4}$$

where V (V) is the applied voltage, J (A·cm^{-2}) is the measured current density, q (C) is the absolute value of the electronic charge, A^* (A·cm^{-2}·K^{-2}) is the Richardson constant which is 110 A·cm^{-2}·K^{-2} for n-type silicon, and k and T are Boltzmann's constant and absolute temperature, respectively.[15]

From the linear fitting of the plots of ln[J/(1-exp(-qV/kT))] vs. V (Figure 3.3) for a representation of a rectifying junction, η can be obtained from the slope (qV/(ηkT)), and $q\phi_{eff}$ can be calculated from the intercept (ln(A^*T^2)-$q\phi_{eff}$/(kT)).

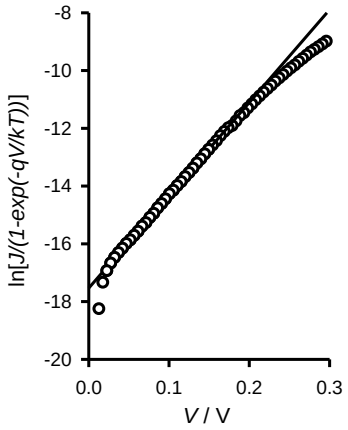

Figure 3.3 Calculation of the effective barrier heights and ideality factor from the linear fitting of the J-V curves: plot of ln[J/(1-exp(-qV/kT))] versus V for a Hg-S-C18|H-Si≡ junction as prepared.

In Figure 3.1(c) we have plotted $q\phi_{eff}$ and η as function of the Hg drop area change ratio (A/A_0). The $q\phi_{eff}$ and η values were 0.83 ± 0.04 eV and 1.16 ± 0.07 at the initial stage, and changed to 0.43 ± 0.01 eV and 2.65 ± 0.05, respectively. In this case, the junction behaves as a resistor, and these values are close to those of the Hg|H-Si≡ junction reported previously.[62] It is also clear that a 10-15% increase in the surface area of the mercury drop leads to complete switching between rectifying and ohmic behavior, when all other conditions (components) are kept unchanged.

3.1.2. Deformation of the Hg Contact

The above results demonstrate that the electrical properties of an Hg-S-C18|H-Si≡ junction can be tuned by simply increasing the Hg drop surface area. However, it is not feasible to reverse the change. Retracting the Hg drop (modified with SAMs) into the syringe would contaminate the remaining Hg inside. Due to the design of gas-tight syringes, it is also difficult to accurately control the expansion of the Hg drop. Therefore, we explored an alternative approach of pressing "down" the syringe to deform the relatively spherical drop into an oblate one and lifting it "up" to return to the spherical shape. We calculated the surface area of the Hg drop according to its shape as shown in Figure 3.1 and Figure 3.4. When the syringe was "up", a spherical shape and equation 3.1 were adopted. At the "down"position, the shape of the Hg drop was oblate and the following equation was used,[69]

$$A_{obl} = 2\pi\left(\frac{d_2}{2}\right)^2 + \frac{\pi(l/2)^2}{(1-l^2/d_2^2)^{1/2}} ln\frac{1+(1-l^2/d_2^2)^{1/2}}{1-(1-l^2/d_2^2)^{1/2}} - \pi\left(\frac{d_1}{2}\right)^2 \quad (3.5)$$

where d_1, l, and d_2 were obtained from the enlarged optical image (40× magnification) (Figure 3.4). The results are shown in Table 2.

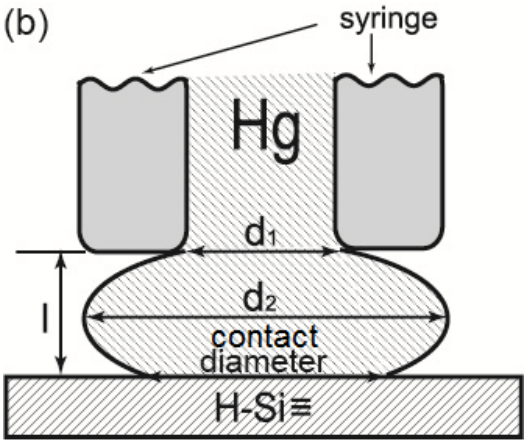

Figure 3.4 Schematic view of the oblate shape of a Hg drop upon pressing down the syringe. (The schematic view is around 25 times larger than the real size of Hg drop.)

Table 3.2 Deformation of Hg drop

contact diameter (mm)	d_1 (mm)	d_2 (mm)	l (10^2 μm)	A_0 (mm^2)	A (mm^2)	A/A_0
0.70±0.04	1.00±0.05	1.51±0.07		6.78±0.61		
1.58±0.08	1.00±0.05	1.99±0.10	0.96±0.05		7.66±0.69	1.13±0.15
1.77±0.09	1.00±0.05	2.08±0.10	0.79±0.04		7.72±0.69	1.14±0.15
2.13±0.11	1.00±0.05	2.34±0.12	0.61±0.03		9.06±0.82	1.24±0.16

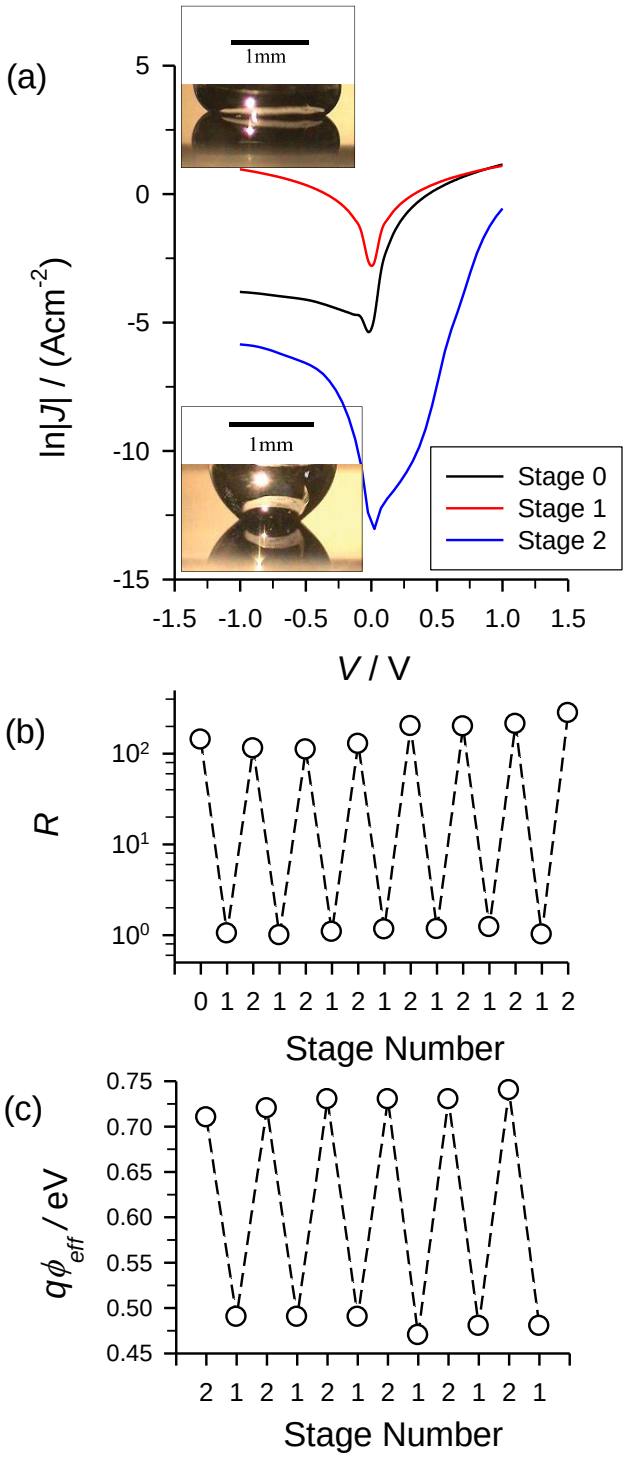

Figure 3.5 (a) Representative current density vs. voltage (*J-V*) plots for Hg-S-C18/H-Si≡ junction upon deforming the Hg drop. (b) Rectification ratio (*R*) and (c) barrier height $q\phi_{eff}$ upon changing the shape of the Hg drop. Stage 0: freshly made Hg-S-C18|H-Si≡ junction; stage 1: "depressed" drop; stage 2: "released" drop.

We found that the *J-V* properties of this junction also changed significantly with the shape change of the Hg drop. This “deformation” process of the Hg contact was monitored by recording several consecutive *J–V* plots in the “up” and “down” positions within 5 min of each other. During this process, the volume of the protruding Hg drop did not change.

In Figure 3.5 (a) we have shown representative *J-V* curves of the initial contact (Stage 0, black line), a “depressed” drop (Stage 1, red line) and a “released” drop (Stage 2, blue line) of a Hg-S-C18|H-Si≡ junction. Upon pressing down the mercury drop, the initially asymmetric *J-V* curve significantly changed its appearance: it became symmetric (the current at forward bias is similar to that at reversed bias). This indicates that the junction switched from rectifying (Stage 0) to ohmic (Stage 1), similar to the volume expansion result shown in Figure 3.1 (a). However, we noticed that the current density was similar in both Stage 0 and Stage 1 at the forward bias (0.5 V to 1.0 V). After releasing the droplet from Stage 1, the *J-V* curve became rectifying again (Stage 2) with lower currents on both reverse and forward biases. Remarkably, the *J-V* curves could be switched between Stage 2 and Stage 1 when the drop was repeatedly pressed down and lifted up.

Figure 3.5 (b) depicts the variation of the rectifying ratio between Stage 1 (depressed drop) and Stage 2 (released drop). This switching experiment was repeatable more than 10 times (7 cycles are shown here) with almost no change of the current density at each stage. The R was almost 1 at Stage 1 and it was at the same magnitude (~ 100) at Stage 2, but the value for each time were not the same. We also noticed that the switching of $q\phi_{eff}$ during the repetition was reproducible. As shown in Figure 3.5 (c), the ohmic stage has a $q\phi_{eff}$ value of 0.46 ± 0.01 eV which is the same as that of an Hg|H-Si≡ junction (0.46 ± 0.05 eV),[62] while that of Stage 2 is 0.75 ± 0.02 eV, which is close to that of an alkyl monolayer-modified junction.[62, 70]

3.1.3. *Electrical Properties of Hg|C12-S-Si≡ Junctions*

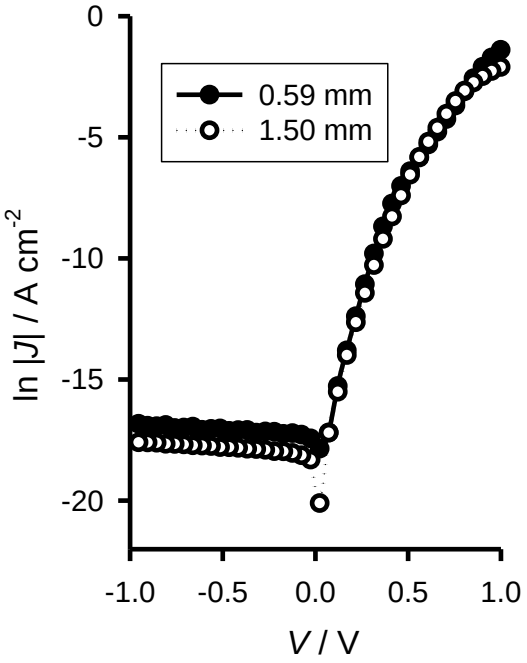

Figure 3.6 Representative current density vs. voltage (*J-V*) plots for Hg|C12-S-Si≡ junction upon enlarging the Hg drop. These junctions showed no changes in their electrical behaviour during both volume expansion and deformation of the Hg contact.

As a control experiment, we tested the junctions modified with covalently bonded dodecanethiolate (C12)-monolayers on silicon (Hg|C12-S-Si≡). We carried out both volume expansion and deformation of the Hg contact to determine whether these processes have any effect on the electrical performance of the junction. As shown in Figure 3.6, the diameter of the mercury drop contact with the silicon surface changed from 0.59 ± 0.03 mm to 1.50 ± 0.08 mm and had little effect on the apparent shape of the *J-V* plot.

3.1.4. Electrochemical Studies of C18SH SAM on Hg

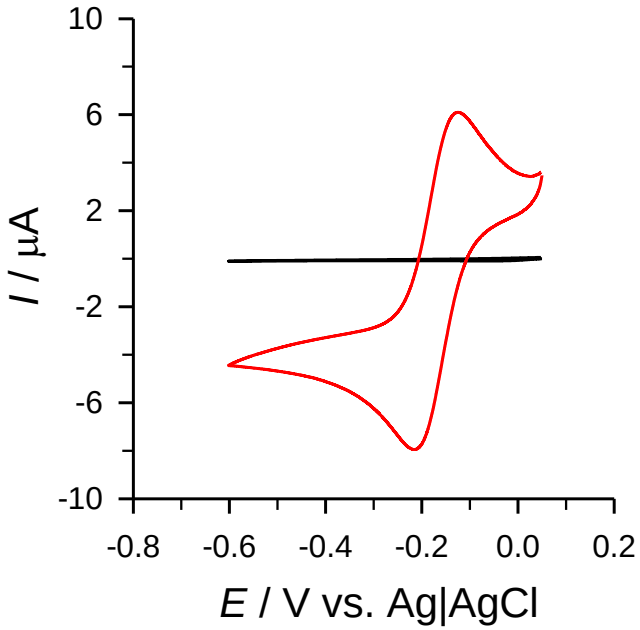

Figure 3.7 Cyclic voltammograms of 5 mM $Ru(NH_3)_6^{3+}$ on a C18 SAM-modified Hg drop before (black line) and after 11% increase of the surface area (red line). The scan rate was 50 mV/s, and the supporting electrolyte was 0.1 M KCl.

To better understand the electrical switching behavior of Hg-SC18|H-Si≡ junctions, we investigated the potential structural change of alkanethiolate SAMs on Hg by using solution-diffused redox centers, e. g. $[Ru(NH_3)_6]^{3+}$. After the Hg drop was immersed in a solution of C18SH, an impermeable and defect-free monolayer was presumably formed on the Hg surface.[36] After forming the SAM, the Hg drop was transferred to a solution containing $[Ru(NH_3)_6]^{3+}$ and tested electrochemically. Figure 3.7 shows the representative CVs obtained before and after the volume of the Hg drop was increased. It was found that when the monolayer was first formed, no redox peak was seen in the curve, indicating that the SAM is densely packed and impermeable to $[Ru(NH_3)_6]^{3+/2+}$. As the drop size gradually increased, the capacitive current became larger, yet no obvious redox peaks were observable. With only a slightly larger change in the drop size (10~11%), redox peaks due to the reduction and re-oxidation of $[Ru(NH_3)_6]^{3+/2+}$ became predominant. It is evident that a minute increase in the surface area of the drop leads to significant structural disruption of the SAM, i.e., facile electron transfer between the solution-diffused redox centers and the electrode occurs,

presumably at the defect sites created by the surface area increase. These results are in fact consistent with previous studies on C18 SAMs formed on traditional hanging mercury drop electrodes.[38-39] Particularly, Bruckner-Lea et al. discovered that upon increasing the surface area of a Hg drop by 6%, the film starts to generate “bare spots,” or defects. Slowinski et al. confirmed that a C18 monolayer remains impermeable until the surface area of the drop has increased by approximately 6.9%.[39] Further expansion (~10.2%) of the drop fractures the monolayer, causing a sharp current increase.[39]

3.1.5. Hypothetical Structural Change of SAMs on Hg Contact

With the additional evidence provided by these electrochemical study, we believe that both the volume expansion and the above shape deformation produce dynamic changes in the structural integrity of the C18 SAM on Hg. As illustrated in Figure 3.8 (a), when the Hg-S-C18|H-Si≡ junction is freshly formed, the alkyl chains of the C18 SAM initially orient themselves nearly perpendicular to the Hg surface before settling into an energetically more favorable tilted orientation.[45, 71-72] As the Hg drop volume increases or pressure is applied, the alkyl chains begin to tilt and aggregate, creating defects in the monolayer (Figure 3.8 (b)).[38-39]The defects gradually propagate due to the mobility of SAMs on such a liquid metal surface. Finally, as shown in Figure 3.8 (c), defects play a dominant role in the junction, allowing the mercury to make direct contact with H-Si≡ which results in the observed change of electronic properties from rectifying to ohmic.

We should also mention the differences in the electrical properties of the junctions by volume expansion and by shape deformation of the Hg drop (beyond reversibility). As shown in Figure 3.2 (a), the current density at forward bias for ohmic contact (A/A_0 = 1.14) is higher than that of the freshly made rectifying junction (A/A_0 = 1.00). Whereas in the pressing/releasing experiment (Figure 3.5 (a)), at forward bias a similar current density is found for both ohmic contact (Stage 1) and rectifying junction (Stage 0). This is probably due to the formation of large bare spots when the volume of the mercury drop is increased. For the deformation experiment, one may expect an uneven distribution of thiol molecules at the interface. Such a difference may help to explain the different behavior at Stage 0 and Stage 2. The much lower current measured at the rectifying Stage 2 may be due to the presence of thiol molecules in a lying-down conformation. Kraack et al. have confirmed that thiol molecules would undergo a

transition from surface-parallel at low coverage to surface-normal orientation at high coverage for a monolayer-covered Hg surface.[34] The alkanethiolate monolayers on the surface of liquid mercury are believed to form strong chemical bonds to Hg which is initially atomically flat and unstructured; strong interactions of the thiol groups with the Hg surface dominate the order of molecules over van der Waals interactions of the alkyl chains.[73] Their inability to recover to an ordered state via simply releasing the pressure may lead to the observed switching between Stage 1 and Stage 2.

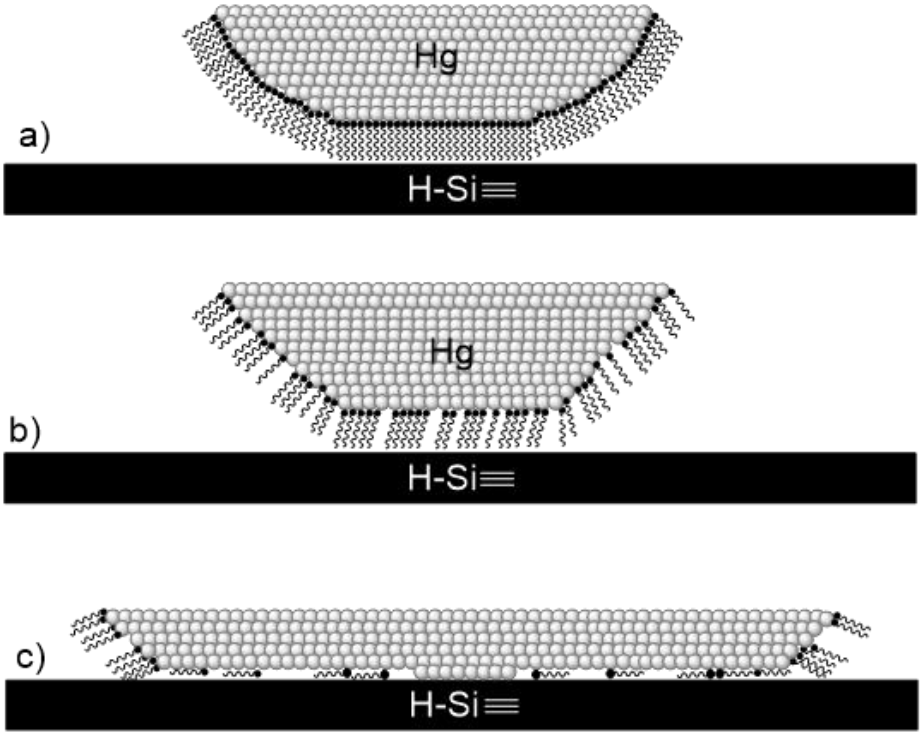

Figure 3.8 Schematic view of the potential structural changes in a C18 SAM on Hg (as top electrode) in contact with H-Si≡: (a) a defect-free junction; (b) alkyl chains tilted and small bare spots created when increasing the surface area of the Hg drop; (c) direct contact between bare Hg and H-Si≡ upon further increasing the surface area.

Although molecular electronic devices are not yet commercially available, the ability to manipulate functional groups of organic molecules by the self-assembly process to satisfy various technological requirements is of fundamental interest.[6] We have discovered that by simply enlarging the volume or deforming the mercury drop, the *J-V* response of these molecular junctions reversibly switches between ohmic and rectifying behavior. Evaluation of the ideality factor and effective barrier height proves

that we can mechanically switch the molecular diode “on” and “off”. The junction formed by a C_{18} SAM-modified Hg junction can be switched “on” and “off” multiple times which shows the ability of the monolayer to recover its ordered conformation and orientation. By and large, this experiment provides a unique approach to study the structural dynamics of molecular assemblies at the solid/liquid interface.

3.2. Electrical Properties of Hg-SAM|H-Si≡ Junctions with Alkanethiols of Different Chain Lengths

To better understand the influence of dynamic structural change of the embedded molecular monolayer on the electrical properties of Hg-SAM|H-Si≡ junctions, I decided to examine a series of alkanethiolate SAMs with different chain lengths. In this set of experiments, no volume enlargement or deformation of the Hg drop was performed. Once the SAM-modified Hg drop contacted the H-Si≡, we left it in the faraday cage, and the solid-state electrical measurements were performed at different time intervals. Here, I define C10SH, C11SH, and C12SH as short chain alkanethiols and C14SH, C16SH, and C18SH as long chain alkanethiols, as they indeed behaved differently in terms of the *J*-*V* properties (as will be described in detail below).

3.2.1. Electrical Behavior of Junctions Formed with Short Chain Alkanethiols

Figure 3.9 depicts a typical set of current density-voltage (*J*-*V*) curves measured with the Hg-S-Cn|H-Si≡ junctions (n = 10, 11, and 12). The logarithmic plots show the exponential dependence of the current density on applied voltage. From the black line in Figure 3.9 (a), we can see that the *J*-*V* curve of the freshly made Hg-S-Cn|H-Si≡ junctions were all asymmetric, suggesting these are rectifying junctions (diode-like). Taking the Hg-S-C10|H-Si≡ junction as an example, the *J*-*V* properties underwent significant changes with a period of 250 min. The current density under reverse bias ($V < 0$) became smaller while the current density under forward bias ($V > 0$) did not change much for the first 50 min (as illustrated in Figure 3.9 (a), black line to pink line) This is rather interesting, as the current density changes under reversed bias, while it remained almost unchanged under forward bias. From 50 to 100 min (Figure 3.9 (a) pink line to

green line), the current density under reverse bias decreased further but the forward bias current density increased slightly. As the time went by, the current density under reverse bias increased together with the forward bias current density, but the extent was much larger for the former (Figure 3.9 (b)). Finally, the *J-V* plot became symmetric (Figure 3.9 (b) dark pink line at 250 min). This is typical for an ohmic junction, i.e., the junction behaves as a resistor. It should be noted that Hg-S-C11|H-Si≡ and Hg-S-C12|H-Si≡ junctions have similar electrical behavior trends as that of Hg-S-C10; this is shown more clearly by examining the rectification ratio.

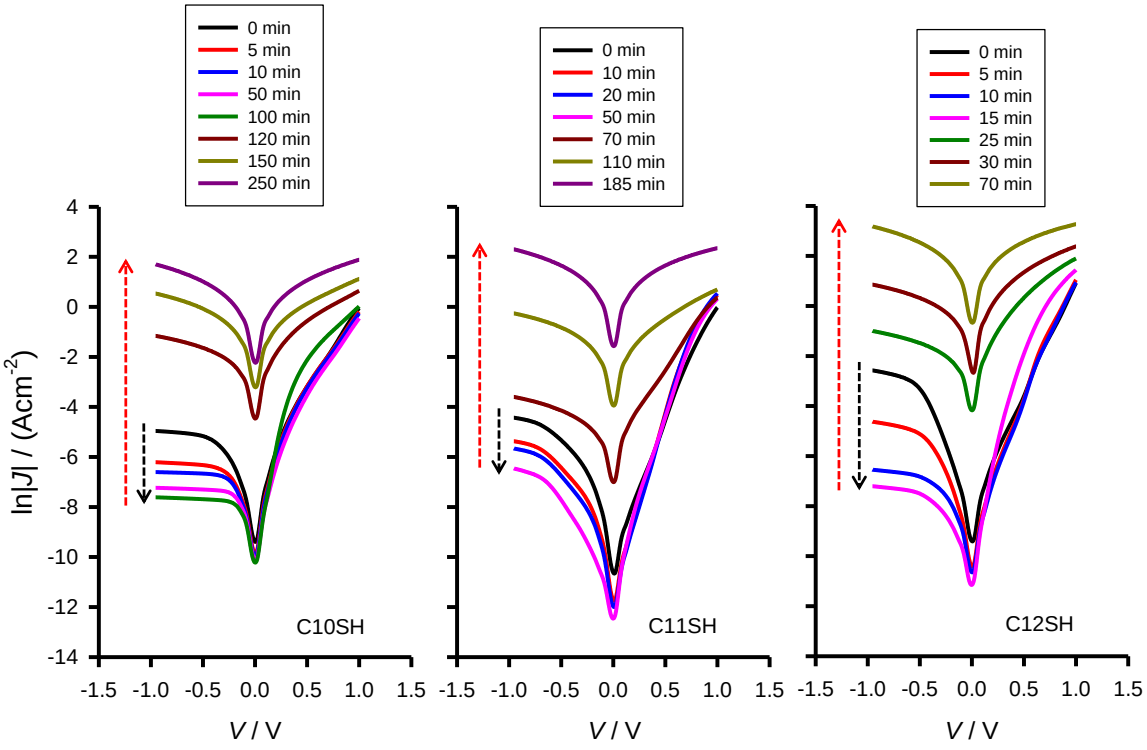

Figure 3.9 Variation of current density-voltage (*J-V*) curves of Hg-S-Cn|H-Si≡ junctions (n = 10, 11, 12) with time. Current density under reverse bias initially decreases with time, as indicated by the black arrow. After longer periods of time, the current densities under both reverse and forward bias increase until the *J-V* curves become symmetric.

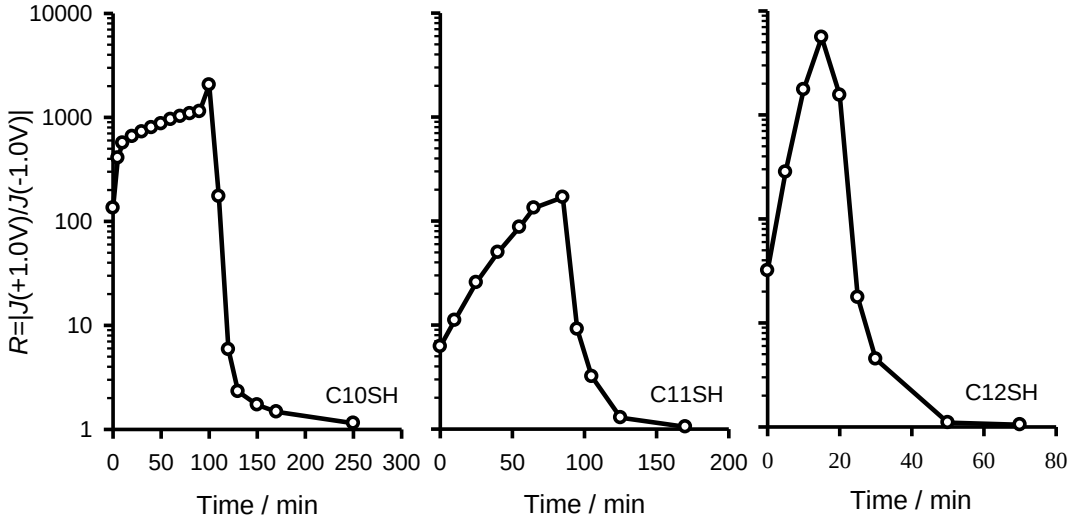

Figure 3.10 Variation of the rectification ratio (*R*) as function of time for the Hg-S-Cn|H-Si≡ (n=10, 11, 12) junctions.

Rectification ratio (*R*) is the comparison of current density at ± 1.0 V as mentioned before. We can see from Figure 3.10 that the *R* values of all three junctions showed an increasing trend for a relatively short time period when the current density went lower under reverse bias. The *R* value went up to a maximum when the reverse bias current density reached a minimum and then dropped to almost unity. When *R* is close to unity, the current densities are identical under both reverse and forward bias, indicative of ohmic behavior.

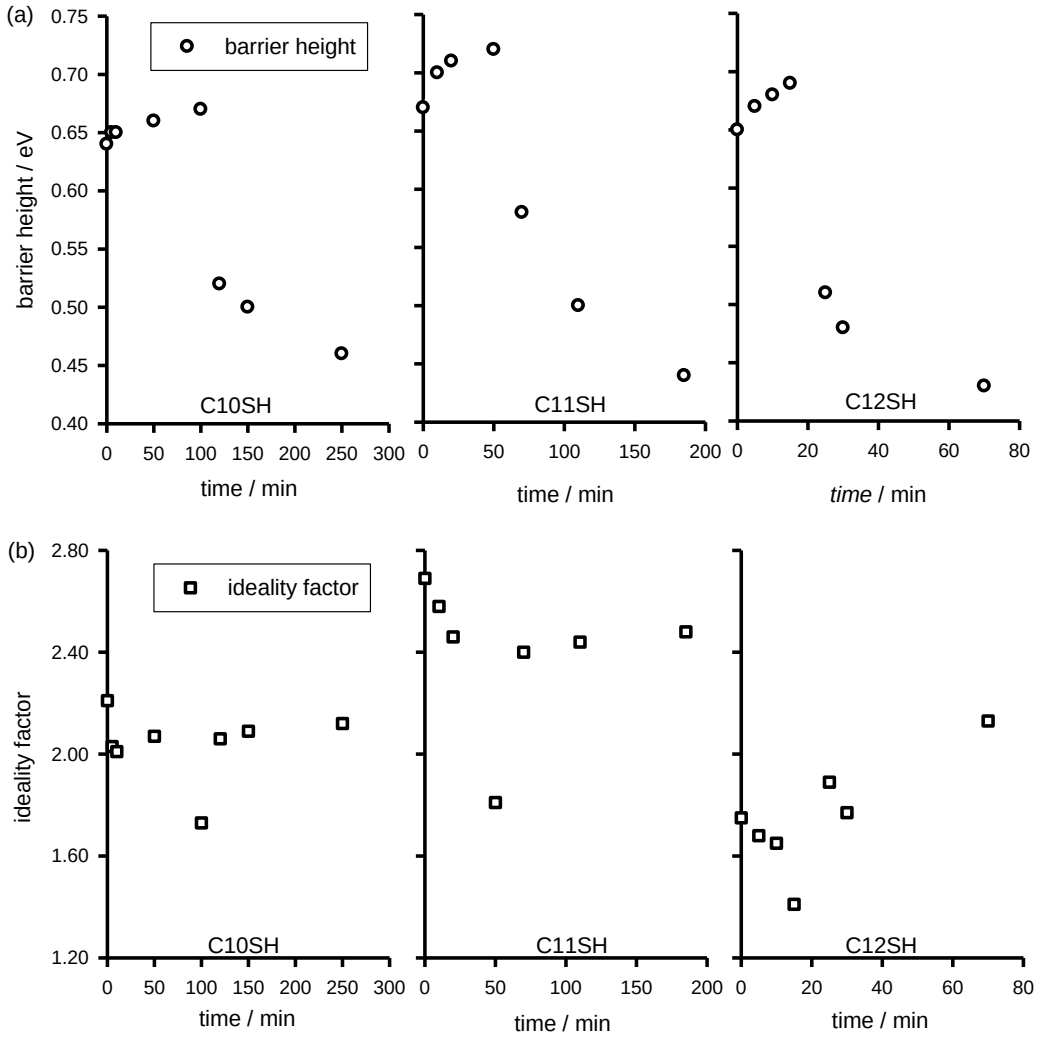

Figure 3.11 (a) Barrier height ($q\phi_{eff}$) (circles) and (b) Ideality factor (η) (squares) as function of time for the alkanethiols junctions prepared from short chain.

Furthermore, the barrier heights ($q\phi_{eff}$) and ideality factors (η) were chosen to demonstrate how the electrical properties changed as function of time for these molecularly modified MS junctions. The calculations of $q\phi_{eff}$ and η are based on the thermionic emission theory as mentioned before. In Figure 3.11 (a) we can see that the barrier heights of all three junctions increased at the same time as R increased, then reached a maximum and decreased to about 0.44±0.02 eV, which is identical to the value for a Hg|H-Si≡ junction. The η (squares) value showed a decreasing trend and reached the minimum when the barrier height reached its maximum. Then it increased to approximately 2.2±0.2 (Figure 3.11 (b)).

3.2.2. *Electrical Behavior of Junctions with Long Chain Alkanethiols*

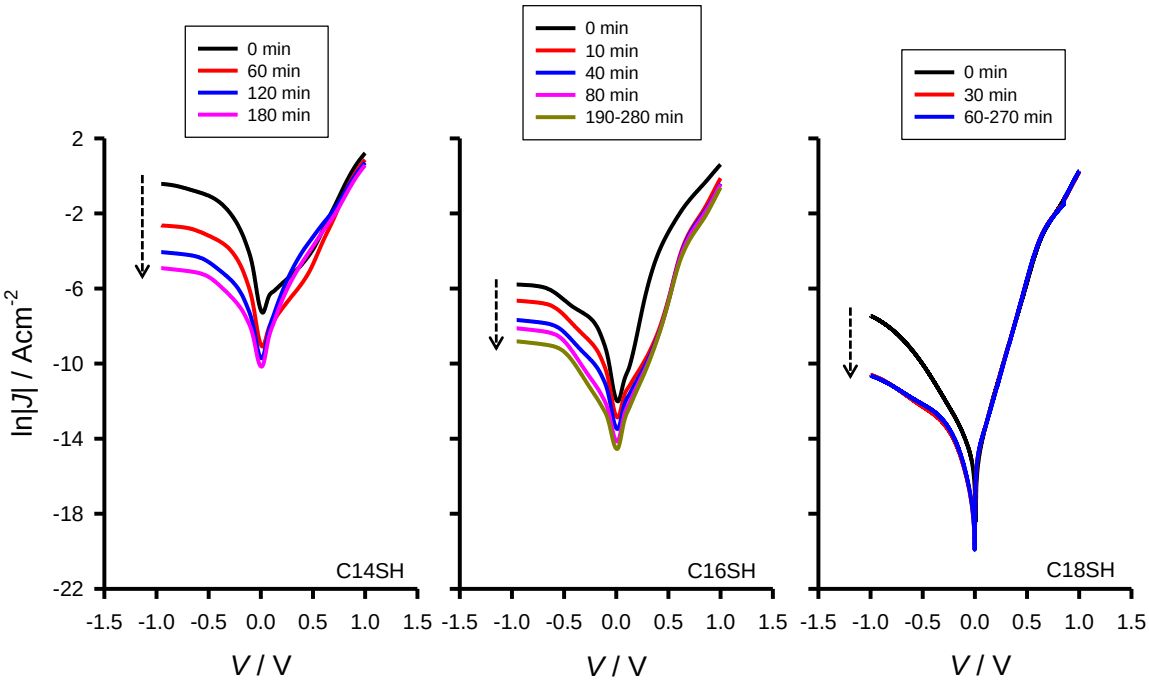

Figure 3.12 Current density-voltage (*J-V*) curves of various Hg-S-Cn|H-Si≡ (n=14, 16, 18) junctions. Current density under reverse bias decreases with time, as indicated by the black arrow.

The *J-V* behavior of the Hg-S-Cn|H-Si≡ junctions prepared with long-chain alkanethiols (n = 14, 16, and 18) is quite different from that of the short-chain ones. The *J-V* curves of Hg-S-Cn|H-Si≡ (n=14, 16, 18) junctions showed rectifying contacts when freshly made (black line in Figure 3.12). Taking the junction Hg-S-C16|H-Si≡ as an example, the current density under both reverse and forward bias decreased after 10 min (shown as red line). With increasing time (from 40 min to 80 min), the current density decreased further under reverse bias, while it remained constant under forward bias. After 190 min, the current densities under both forward and reverse bias became stable. These junctions would not change to ohmic behavior, unlike the short-chain systems.

For a direct comparison with the long-chain junctions, the *R* values were also calculated and are shown in Figure 3.13. It is clear that the *R* values of all three types of junctions increase at first and remain stable afterwards. The calculated $q\phi_{eff}$ and η

values (based on the thermionic emission theory) showed different trends from the short-chain systems as well. As depicted in Figure 3.14, the effective barrier height increased for some time and then remained stable while η decreased (Hg-S-C14|H-Si≡ and Hg-S-C16|H-Si≡) or remained almost unchanged (Hg-S-C18|H-Si≡).

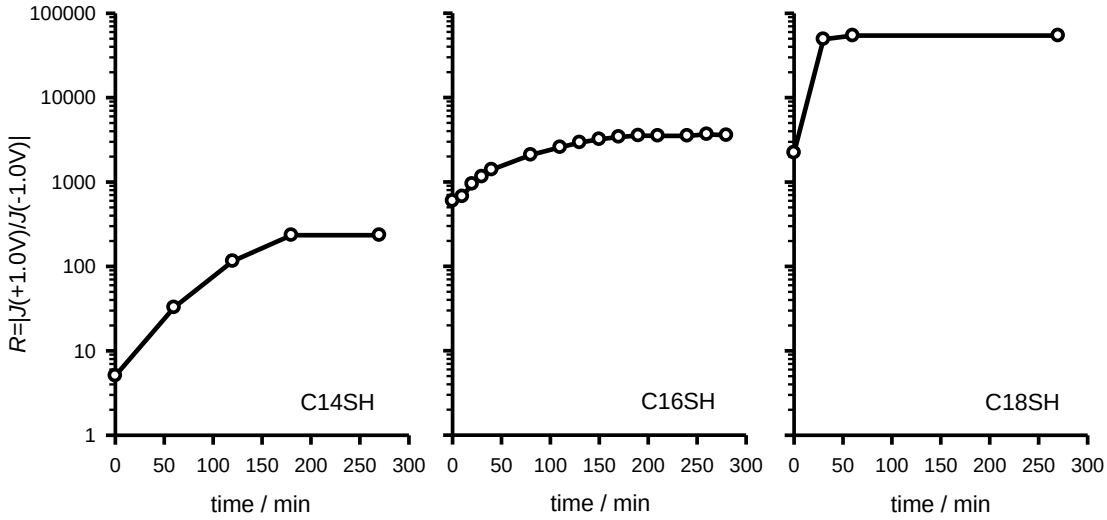

Figure 3.13 Rectification ratio (*R*) as function of time for the long-chain Hg-S-Cn|H-Si≡ junctions.

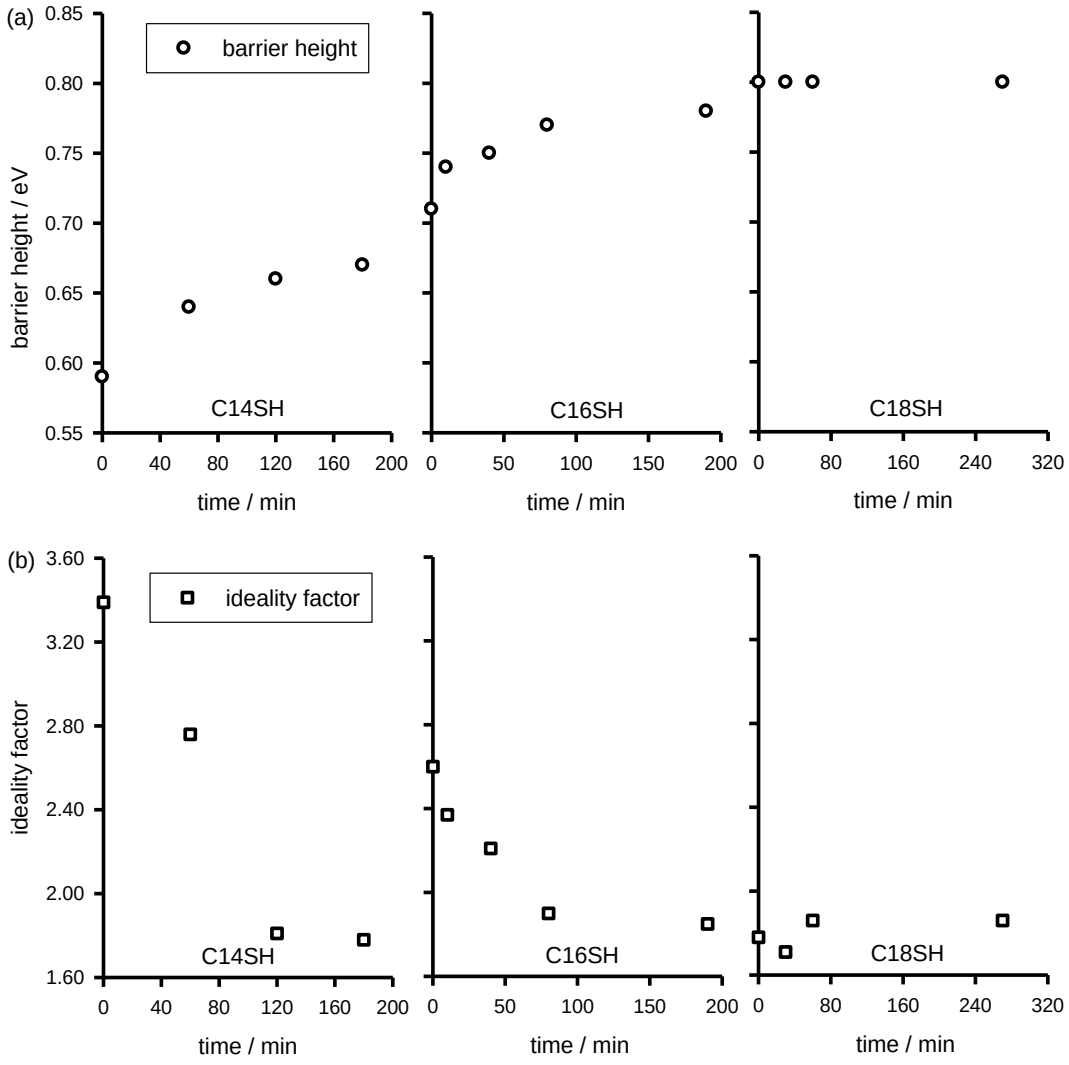

Figure 3.14 (a) Barrier hight ($q\phi_{eff}$) (circles). (b) Ideality factor (η) (squares) as function of time for the alkanethiols junctions prepared from long chain.

3.2.3. Discussion

The *J-V* behaviors of short-alkyl-chain and long-alkyl-chain alkanethiolate SAMs on Hg differed substantially. The short chain Hg-S-Cn|H-Si≡ (n=10, 11, 12) junctions demonstrated an initial increase in rectifying property (*R* is increasing) with time, however with additional time the contact eventually becomes ohmic ($R \approx 1$). This differs from the long chain systems which showed a steady rise in rectifying behavior before being stabilized.

It is believed that by immersing a Hg drop in an alkanethiol solution for 10 min, a high-coverage SAM is formed on the surface.[65] To determine whether the immersion time was responsible for the more rectifying behavior, we immersed the Hg drop in C11SH for a longer period of time (i.e. 5 h). We found that the Hg-S-C11|H-Si≡ junction behaved the same way as immersion in alkanethiol for 10 min; the rectifying behavior increased initially before decreasing until becoming ohmic. For each alkanethiol, at least 15 junctions were made, and the contact area error was within ±10%. When the electrical signal was measured, the scan rate was set at 0.1 V/s. We also did continous scans and discovered that the time for the junction to change to an ohmic contact did not change substantially. Therefore, the rather unique electrical properties for different chain lengths appear to be mainly due to the balance between the chemisorption of head groups on the substrate and the van-der-Waals forces between the alkyl chains.

For the short-chain SAMs formed on the Hg surface, the first and most important process is chemisorption. The interaction between head groups and substrate often dominates the molecular structure of the film. In case of the sulfur atom of the thiol interacting with the Hg substrate, the bond energy is about 128 kJ/mol.[23] This is much larger than hydrocarbon chains physisorbing on the mercury surface with a heat of adsorption $\Delta H \approx 5$ kJ/mol per CH_2 group and the adsorption energy of 5.4 kJ/mol of per methyl head group.[74] For short alkanethiols, the difference in adsorption energy between a CH_2 chain and the CH_3 functional group is too small to make the molecules stand up (Figure 3.15 (a)). However, as a result of the exothermic head group-substrate interactions, molecules try to occupy every available binding site on the surface, and in this case they push together molecules that have already occupied the available sites. Therefore, the alkyl chains rearrange themselves in a more ordered way (Figure 3.15 (b)), which results in a larger separation between Hg and H-Si≡ and an increase of the barrier height of the junction. The current density decrease under reverse bias is mainly due to this barrier height increase which the electrons moving from the metal to the semiconductor side must overcome. If the effective barrier is higher, fewer electrons will overcome it under reverse bias. The current density under forward bias is not affected by the effective barrier height since as previously mentioned, the electrons move from the semiconductor to the metal (Figure 1.2) over the built-in potential which is reduced by the forward bias. Finally, the inter-chain van-der-Waals interactions of short chain thiols

(< 40 kJ/mol) is not large enough to keep the molecules in their original positions. Besides, SAMs on a Hg surface reduce the surface tension of bare Hg.[74] This smaller surface tension makes the short alkanethiols gather together, and the small van der Waals forces cause the SAMs to separate. Bare Hg spots appear and touch H-Si≡ due to these two effects, thereby generating Hg|H-Si≡ junctions which behave as resistors (Figure 3.15 (c)). Here we should mention that during the entire process the contact area between SAM-modified Hg and H-Si≡ has not changed.

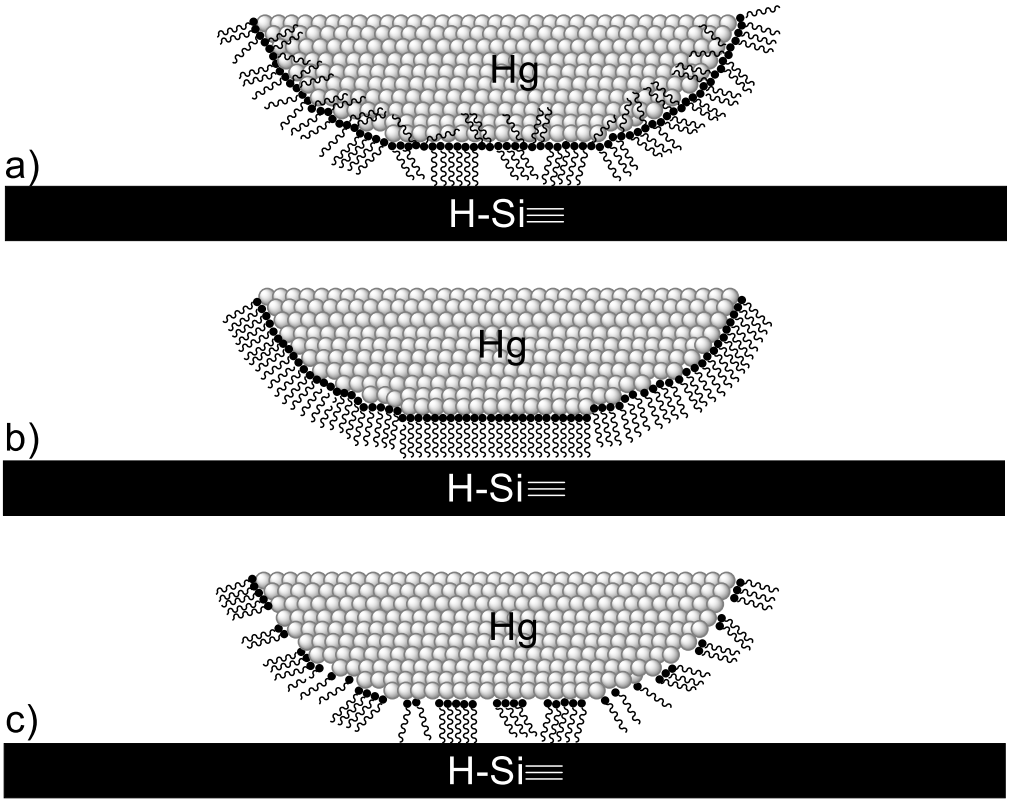

Figure 3.15 (a) SAMs originally formed on the Hg surface. (b) The molecules are packed more orderly. (c) Formation of Hg|H-Si≡ junctions at the defects (bare spots) after rearrangement of the alkanethiols behaving as resistors.

As to long alkanethiols on Hg, at the beginning of the C14, C16 and C18 chemisorption process on Hg, the alkyl chains arrange to form more ordered monolayers than short-chain alkanethiols. With time, the long chain alkanethiols rearrange to form densely packed monolayers due to larger van der Waals forces, causing the current density under reverse bias to be lower than that of the originally formed junction. These junctions remain as diodes because the van der Waals forces between the alkyl chains

are large enough to maintain a densely packed and impermeable monolayer on the Hg surface (Figure 3.15 (b)).

3.3. Preliminary Studies of Hg|fullerene-Si≡ Junctions

To further investigate the electrical properties of organic monolayers, buckminsterfullerene (C_{60}) was immobilized on Si to construct gold (Au)|C60-Si≡ junctions. C_{60} is a group of carbon atoms with a relatively large, spherical shape. It consists of 12 pentagonal and 20 hexagonal rings. All carbon atoms are sp^2 hybridized. Its unique structure, chemical and physical properties, and several promising applications in semiconductor technology have been studied recently[75]. The direct immobilization of C_{60} on Si(111) substrates has been confirmed with scanning tunneling microscopy[76], and the indirect immobilization of C_{60} on Si (100) involves conditions such as prefunctional groups[77]. As each C_{60} consists of a large number of carbon atoms with different types of bonds, their binding to a semiconductor surface is quite complicated. Therefore, we placed C_{60} on top of H-Si≡ with a linker molecular monolayer that bears NH_2- groups.

Initially we studied the fullerene-modified silicon surface by using X-ray photoelectron spectroscopy (XPS), *J-V* charaxterization with Hg as contact electrode, ellipsometry and contact angle. Figure 3.16 shows our XPS data of the silicon surface after modification with propargylamine ($HC{\equiv}C\text{-}CH_2\text{-}NH_2$) and C60, respectively. The atomic percentage of carbon (C1s) is found to increase from 16.26 to 25.28, and that of nitrogen (N1s) decreases from 3.03 to 1.68 (from silicon modified with $HC{\equiv}C\text{-}CH_2\text{-}NH_2$ to C_{60}-functionalized silicon). The Si 2p 3/2 peak due to Si-C species is found in the 100-eV binding energy region.

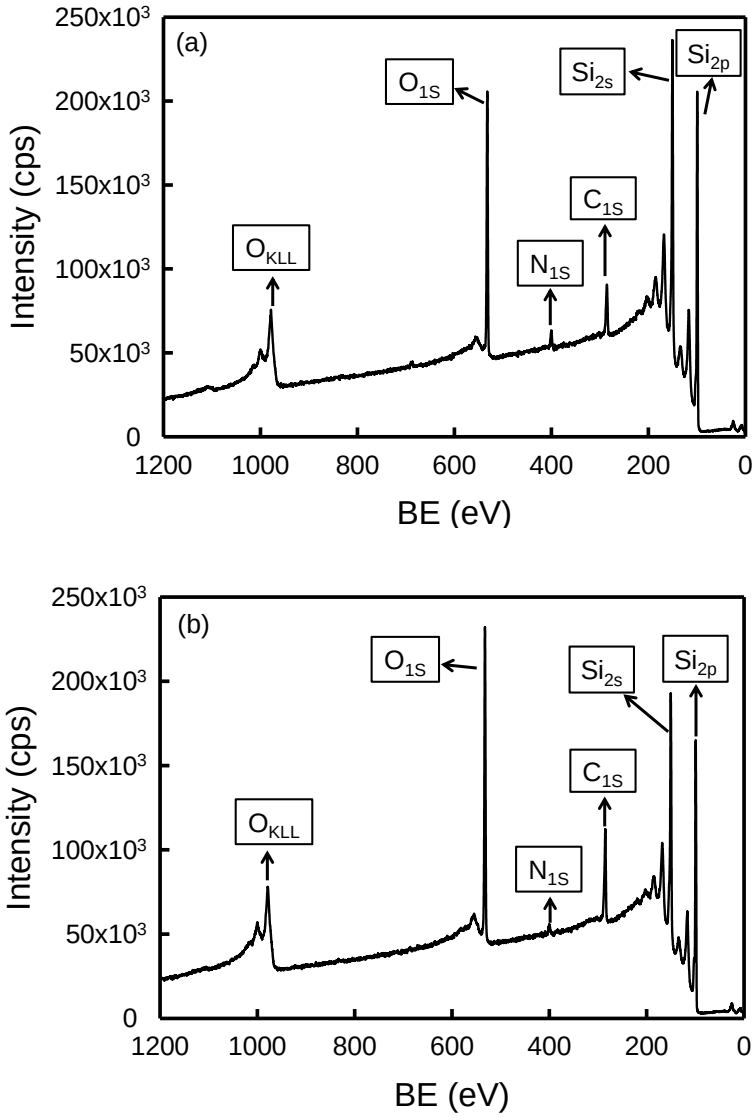

Figure 3.16 XPS scan of a Si substrate modified with $HC{\equiv}C\text{-}CH_2\text{-}NH_2$ (a) and of a C60-functionalized silicon substrate (b).

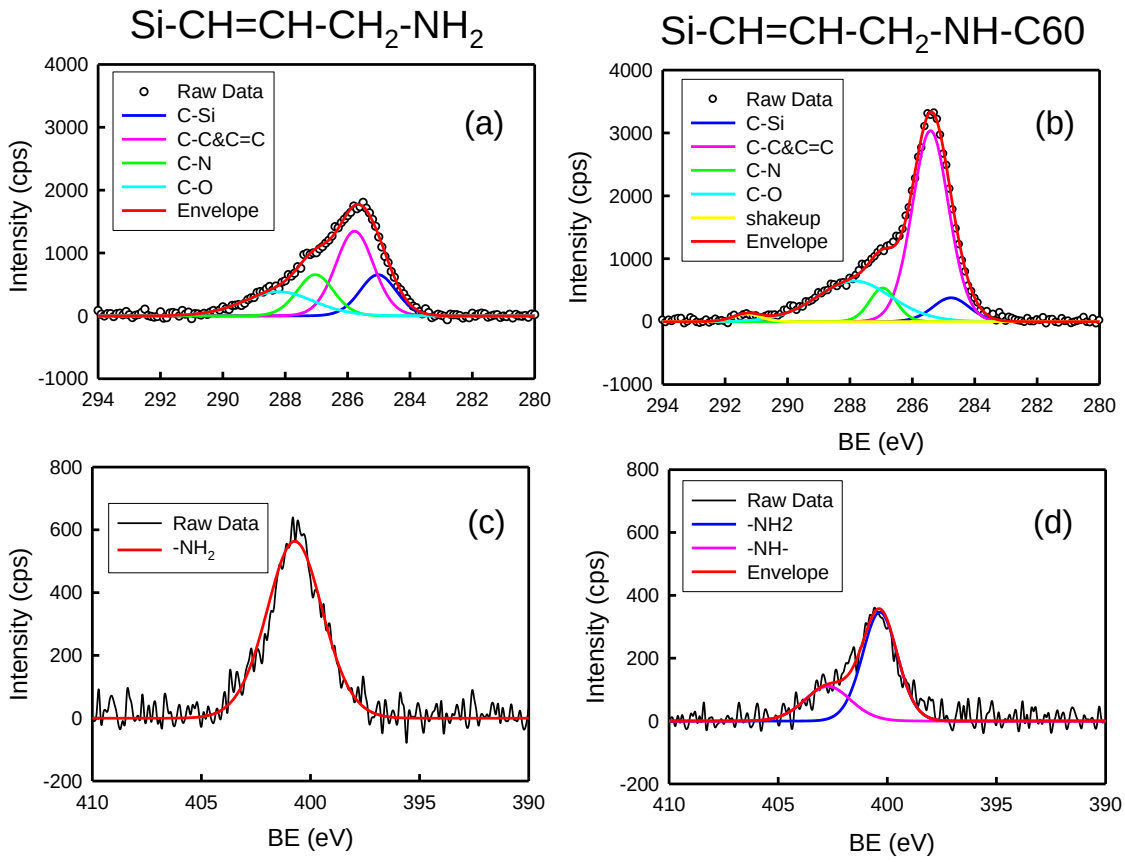

Figure 3.17 High-resolution XPS scans showing the C1s and N1s regions. (a) and (b) are C1s peaks of HC≡C-CH_2-NH_2 modified Si substrate and of a C60-functionalized silicon substrate. (c) and (d) are N1s peaks of HC≡C-CH_2-NH_2 modified Si substrate and a C60-functionalized silicon substrate.

The HC≡C-CH_2-NH_2 SAM and the C_{60}-modified SAM on silicon surface were also characterized by high-resolution XPS (Figure 3.17). The C1s peak for the HC≡C-CH_2-NH_2 monolayer appears between 284.0 eV and 289.0 eV. This region is rather wide due to the multiplex substitutions (e.g., C-Si, C-C & C=C, C-N and C-O bonds). The peaks at 285.1eV and 285.8 eV are assigned to the C-Si and C-C & C=C bonds after the reaction of HC≡C-CH_2-NH_2 with the H-Si≡ surface. The C-N bond is at 287.0 eV,[78] and the C-O bond at 288.2 eV could originate from partial oxidation of the silicon sample after reaction with C_{60}. Compared to spectrum (a), the intensity of the C1s peak at 287.0 eV (C-N) in spectrum (b) is reduced from 19.9% to 7.5 %, and the intensity of C-C and C=C in spectrum (b) is increased from 30.0% to 58% because of the C_{60} attachment to the surface. The ratio of C-N to C-Si is 1.01 in spectrum (a) and 1.03 in spectrum (b). In spectrum (b) the additional C1s shake-up peak at 291.3 eV is attributed to the π-π*

transition, indicating that the C_{60} molecules are attached to the surface.[78-79] Comparing the N1s spectrum of the HC≡C-CH_2-NH_2 SAM (c) and the C_{60} attached surfaces (d), the total N1s intensity is decreased by 1.90%, which may be due to damage caused by the C_{60} reaction with primary amino groups or to the screening effect of the C_{60} molecules. In spectrum (d), the main N1s XPS peak at 400.3 eV is assigned to the primary amino group in the HC≡C-CH_2-NH_2 SAM. The peak at 402.7 is assigned to secondary amino groups directly bound to C_{60} molecules. The NH_2/NH peak area ratio is around 7:3, indicating that about 30% of the primary amino groups react with C_{60} molecules on the surface.

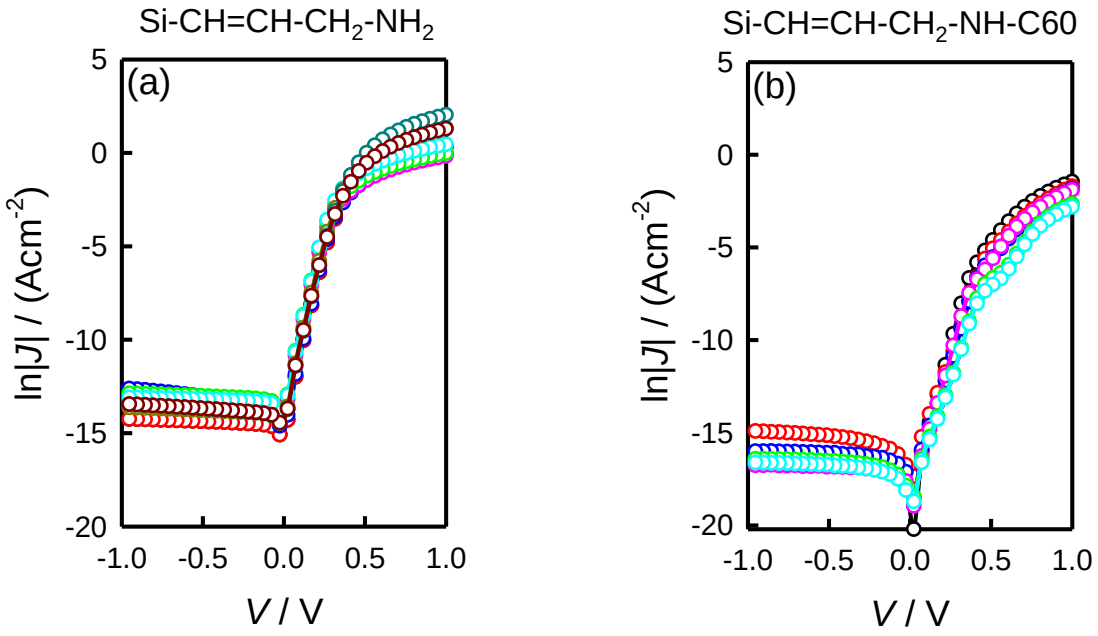

Figure 3.18 Current density-voltage (*J-V*) curves of HC≡C-CH_2-NH_2 SAM-modified silicon surface (a) and C60-functionalized silicon surface (b) with a Hg drop as the top contact electrode.

In Figure 3.18 (a) we show the J-V properties of the HC≡C-CH_2-NH_2 SAM-modified silicon surface with Hg as the top contact electrode. Seven different junctions were measured to show the reproducibility and stability of thus prepared supermolecular junctions. Based on the thermionic emission theory explained before, the ideality factors and barrier heights calculated from these *J-V* curves are 1.04 ± 0.02 and 0.77 ± 0.02 eV,

respectively. In comparison, for the C_{60}-functionalized silicon the ideality factor has increased to 1.44 ± 0.20 and the barrier height to 0.86 ± 0.03 eV. The binding of C_{60} molecules certainly increases the distance between Hg and the silicon surface, although C60, as a big molecule, is unlikely to form a densely packed monolayer. In addition, C60 with a band gap of 1.7 eV is a semiconductor itself, which may change the barrier height of thus formed junctions.

4. Conclusions and Future Work

4.1. Conclusions

My research work has focused on a simple approach of manipulating "metastable" Hg|monolayer|Si junctions. I have discovered that by simply enlarging the volume or deformation the mercury drop, the *J*–*V* response of these molecular junctions changes significantly (for example, from rectifying to ohmic) and more importantly, such switching behavior is reversible and reproducible. This is an example for switching the junction behavior without any complicated modification. The conversion of diodes and resistors is important in electronic applications. It is impossible to change the electrical properties of an Hg|R-Si≡ junction once it has formed by volume expansion and deformation of Hg contact because the monolayer formed on the silicon surface via Si-S bonding is densely packed and robust, such that Hg cannot contact H-Si≡. Furthermore, the formed Hg-S-C18|H-Si≡ junction can be switched "on" (ohmic) and "off" (rectifying) more than ten times, indicating the ability of the monolayer to recover to an ordered state.

The effects of SAMs formed on Hg surfaces with alkyl groups of different chain lengths were also investigated. I found that metal-monolayer-semiconductor junctions formed by short alkanethiols behave as diodes initially, and with time, the rectification ratio increases. It is believed that this is mainly due to reaction of the metal with the thiol group, whose interactions dominate the structure of monolayers at the beginning. As time goes by, the rectifying ratio drops to unity, indicating that the junctions have become ohmic. This likely occurs because the van der Waals forces between the alkyl chains are not large enough for the molecules to sustain an ordered monolayer, thereby leaving defects in the layer. These defects, usually bare Hg spots, can be in direct contact with the H-Si≡ substrate, and resulting in the formation of ohmic contacts. In comparison, the junctions formed from long alkanethiols show increasing rectifying behavior which eventually becomes stable, with no signs of switching to ohmic behavior.

It is thought that, unlike short alkanethiols, the longer chains have much larger Van der Waals forces among themselves enabling the molecules to maintain the monolayer order and resulting in a defect-free junction.

4.2. Future Work

For the monolayer on the Hg electrode, we did different alkyl chain length alkanethiols. Then if we assembly the alkanethiols on the silicon side, we can have a better understanding of how the barrier height is generated in this kind of metal-monolayer-semiconductor junctions. However, there are some difficulties in assembling the monolayer on it. As we tried making Hg|C12-S-Si≡ junctions, we need to use 500 mM dodecanethiol in decane. If we lowered the concentration, the monolayer couldn't be formed on the silicon surface. Besides, for longer chain alkanethiols such as C18SH, it was quite difficult to get a uniform monolayer with the methyl group on top. When we did the experiment, the contact angle of it was around 85° whereas for a uniform C12-S-Si≡ substrate, the contact angle was around 110°. The monolayer modified Si surface could be analyzed by atomic force microscope to find if there is any defects in the monolayer. What's more, we could use other methods to form an alkanethiolate monolayer on top of Si surface.

Other than forming a monolayer on the silicon substrate, we can also use alkanedithiols to assembly on top of the Si surface. The challenge for this approach is to control the experiment conditions that only one layer of alkanedithiols is formed on the Si surface. The generated Hg-S-Cn-S-Si≡ junctions are important on better understanding of whether the chemical bonds playing any role in the electrical measurement of the system. If the chemical bonds as we predicted, play a role in the current transfer, then the current density for Hg-S-Cn-S-Si≡ junctions should be higher than Hg|CH_3-Cn-S-Si≡ junctions.

I have already completed the first two steps on the fullerene project and expect to further explore it. Once a fullerene monolayer is formed, we are going to substitute a Hg contact for a gold contact formed by thermal evaporation. Au is a more favorable contact than Hg as it is physically, mechanically more inert. Ballistic electron emission

microscopy (BEEM) will be used to measure the nanoscale electrical properties of thus formed molecular junctions. As the scanning tunneling microscopy (STM) tip moves from, for example, the apex of an Au-coated C60 molecule down its “slope”, the measured BEEM current is expected to change significantly. This will provide us with an additional means to tune the junction properties. In addition to C60, a variety of carbon-based nanostructures, like single-layer carbon nanotubes and graphene sheets can also react with primary amino groups. This will allow us to study the electrical properties of these novel molecular MS junctions.

References

1. Cui, Y.; Zhong, Z.; Wang, D.; Wang, W. U.; Lieber, C. M., High Performance Silicon Nanowire Field Effect Transistors. *Nano Lett.* **2003,** *3*, 149.

2. Dai, H., Carbon Nanotubes: Synthesis, Integration, and Properties. *Acc. Chem. Res.* **2002,** *35*, 1035.

3. Zhang, Y.; Ichihashi, T.; Landree, E.; Nihey, F.; Iijima, S., Heterostructures of Single-Walled Carbon Nanotubes and Carbide Nanorods. *Science* **1999,** *285*, 1719.

4. Khan, M. A.; Kuznia, J. N.; Bhattarai, A. R.; Olson, D. T., Metal semiconductor field effect transistor based on single crystal GaN. *App. Phys. Lett.* **1993,** *62*, 1786.

5. Waltenburg, H. N.; Yates Jr., J. T., Surface Chemistry of Silicon. *Chem. Rev.* **1995,** *95*, 1589.

6. Bernasek, S. L., Can We Understand the Molecule in Molecular Electronics? *Angew. Chem. Int. Ed.* **2012,** *51*, 9737.

7. Braun, F., Über die Stromleitung durch Schwefelmetalle. *Ann. Phys. Chem.* **1874,** *153*, 556.

8. Bose, J. C. U.S. Patent. **1904**, 775-840.

9. Torrey, H. C.; Whitmer, C. A., *Crystal Rectifyier*. McGraw-Hill: **1948**.

10. Koscienlniak, W. C.; Pelouard, J. L.; Littlejohn, M. A., Dynamic Behavior of Photocarriers in a GaAs Metal-semiconductor-metal Photodetector with Sub-half-micron Electrode Pattern. *App. Phys. Lett.* **1989,** *54*, 567.

11. Schottky, W.; Stromer, R.; Waibel, F., *Hochfrequenztechnik* **1931,** *37*, 162.

12. Schottky, W., Halbleitertheorie der Sperrschicht. *Naturwissenschaften* **1938,** *26*, 843.

13. Mott, N. F., Note on the Contact between a Metal and an Insulator or Semiconductor. *Proc. Camb. Phil. Soc.* **1938,** *34*, 568.

14. Neaman, D. A., *Semiconductor physics and devices: basic principles*. 3rd ed.; McGraw-Hill, **2003**.

15. Sze, S. M., *Physics of semiconductor devices*. 2nd Ed. ed.; John Wiley & Sons, **1981**.

16. Ulman, A., *An Introduction to Ultrathin Organic Films: From Langmuir-Blodgett to Self-Assembly*. Academic Press: Boston, **1991**.

17. Porter, M. D.; Bright, T. B.; Allara, D. L.; Chidsey, C. E. D., Spontaneously Organized Molecular Assemblies. 4. Structural Characterization of n-Alkyl Thiol Monolayers on Gold by Optical Ellipsometry, Infrared Spectroscopy, and Electrochemistry. *J. Am. Chem. Soc.* **1987,** *109*, 3559.

18. Strong, L.; Whitesides, G. M., Structures of Self-Assembled Monolayer Films of Organosulfur Compounds Adsorbed on Gold Single Crystals: Electron Diffraction Studies. *Langmuir* **1988,** *4*, 546.

19. Chidsey, C. D. E.; Loiancono, D. N., Chemical Functionality in Self-assembled Monolayers: Structural and Electrochemical Properties. *Langmuir* **1990,** *6*, 682.

20. Xia, Y.; Whitesides, G. M., Soft Lithography. *Angew. Chem. Int. Ed.* **1998,** *37*, 550

21. Wilbur, J. L.; Kumar, A.; Biebuyck, H. A.; Kim, E.; Whitesides, G. M., Microcontact Printing of Self-assembled Monolayer. *Nanotechnology* **1996,** *7*, 452.

22. Schreiber, F., Structure and Growth of Self-assembling Monolayers. *Prog. Surf. Sci.* **2000,** *65*, 151.

23. Lavrich, D. J.; Wetterer, S. M.; Bernasek, S. L.; Scoles, G., Physisorption and Chemisorption of Alkanethiols and Alkyl Sulfides on Au(111). *J. Phys. Chem. B* **1998,** *102*, 3456.

24. Laibinis, P. E.; Hickman, J. J.; Wrighton, M. S.; Whitesides, G. M., Orthogonal Self-Assembled Monolayers: Alkanethiols on Gold and Alkane Carboxylic Acids on Alumina. *Science* **1989,** *245*, 845.

25. Dubois, L. H.; Nuzzo, R. G., Synthesis, Structure, and Properties of Model Organic Surfaces. *Ann. Rev. Phys. Chem.* **1992,** *43*, 437.

26. Delamarche, E.; Michel, B.; Biebuyck, H. A.; Gerber, C., Golden Interfaces: The Surface of Self-assembled Monolayers. *Adv. Mater.* **1996,** *8*, 719.

27. Bain, C. D.; Troughton, E. B.; Tao, Y. T.; Evall, J.; Whitesides, G. M.; Nuzzo, R. G., Formation of Monolayer Films by the Spontaneous Assembly of Organic Thiols from Solution onto Gold. *J. Am. Chem. Soc.* **1989,** *111*, 321.

28. W. Pan; C. J. Durning; Turra, N. J., Kinetics of Alkanethiol Adsorption on Gold. *Langmuir* **1996,** *12*, 4469.

29. R. Yamada; H. Wano; Uosaki, K., Effect of Temperature on Structure of the Self-Assembled Monolayer of Decanethiol on Au(111) Surface. *Langmuir* **2000,** *16*, 5523.

30. Bensebaa, F.; Voicu, R.; Huron, L.; Ellis, T. H., Kinetics of Formation of Long-Chain n-Alkanethiolate Monolayers on Polycrystalline Gold. *Langmuir* **1997,** *13*, 5335.

31. Tidswell, I.; Ocko, B.; Pershan, P.; Wasserman, S.; Whitesides, G.; Axe, J., X-ray Specular Reflection Studies of Silicon Coated by Organic Monolayers (Alkylsiloxanes). *Phys. Rev. B* **1990,** *41*, 1111.

32. Plueddemann, E. P., *Silane Coupling Agents*. 2nd Ed. ed.; Plenum Press: New York and London, **1991**.

33. Edinger, K.; Goelzhaeuser, A.; Demota, K.; Woell, C.; Grunze, M., Formation of Self-assembled Monolayers of n-Alkanethiols on Gold: a Scanning Tunneling

Microscopy Study on the Modification of Substrate Morphology. *Langmuir* **1993,** *9*, 4.

34. Kraack, H.; Ocko, B. M.; Pershan, P. S.; Sloutskin, E.; Deutsch, M., Structure of a Langmuir Film on a Liquid Metal Surface. *Science* **2002,** *298*, 1404.

35. Li, T. T. T.; Weaver, M. J., Intramolecular Electron Transfer at Metal Surfaces. 4. Dependence of Tunneling Probability upon Donor-Acceptor Separation Distance *J. Am. Chem. Soc.* **1984,** *106*, 6107.

36. Demoz, A.; Harrison, D. J., Characterization and Extremely Low Defect Density Hexadecanethiol Monolayers on Mercury Surfaces. *Langmuir* **1993,** *9*, 1046.

37. Brucknerlea, C.; Janata, J.; Conroy, J.; J.;, P.; Caldwell, K., Scanning Tunneling Microscopy on a Mercury Sessile Drop. *Langmuir* **1993,** *9*, 3612.

38. Brucknerlea, C.; Kimmel, R. J.; Janata, J.; Conroy, J. F. T.; Caldwell, K., Electrochemical Studies of Octadecanethiol and Octanethiol Films on Variable Surface Area Mercury Sessile Drops. *Electrochim. Acta* **1995,** *40*, 2897.

39. Slowinski, K.; Chamberlain, R. V.; Miller, C. J.; Majda, M., Through-Bond and Chain-to-Chain Coupling. Two Pathways in Electron Tunneling through Liquid Alkanethiol Monolayers on Mercury Electrodes. *J. Am. Chem. Soc.* **1997,** *119*, 11910.

40. Slowinski, K.; Chamberlain, R. V.; Bilewicz, R.; Majda, M., Evidence for Inefficient Chain-to-Chain Coupling in Electron Tunneling through Liquid Alkanethiol Monolayer Films on Mercury *J. Am. Chem. Soc.* **1996,** *118*, 4709.

41. Slowinski, K.; Slowinska, K. U.; Majda, M., Electron Tunneling Across Hexadecanethiolate Monolayers on Mercury Electrodes: Reorganization Energy, Structure, and Permeability of the Alkane/Water Interface. *J. Phys. Chem. B* **1999,** *103*, 8544.

42. Stevenson, K. J.; Mitchell, M.; White, H. S., Oxidative Adsorption of n-Alkanethiolates at Mercury. Dependence of Adsorption Free Energy on Chain Length. *J. Phys. Chem. B* **1998,** *102*, 1235.

43. Muskal, N.; Turyan, I.; Mandler, D., Self-assembled Monolayers on Mercury Surfaces. *J. Electroanal. Chem.* **1996,** *409*, 131.

44. Muskal, N.; Mandler, D., Thiol Self-assembled Monolayers on Mercury Surfaces: the Adsorption and Electrochemistry of ω-Mercaptoalkanoic Acids. *Electrochim. Acta.* **1999,** *45*, 537.

45. Kraack, H.; Tamam, L.; Sloutskin, E.; Deutsch, M.; Ocko, B. M., Alkyl-thiol Langmuir Films on the Surface of Liquid Mercury. *Langmuir* **2007,** *23*, 7571.

46. Magnussen, O. M.; Ocko, B. M.; Deutsch, M., X-Ray Reflectivity Measurements of Surface Layering in Liquid Mercury. *Phys. Rev. Lett.* **1995,** *74*, 4444.

47. Kolthoff, I. M.; Barnum, C., The Anodic Reaction and Waves of Cysteine at the Dropping Mercury Electrode and at the Platinum Micro Wire Electrode. *J. Am. Chem. Soc.* **1940,** *62*, 3061.

48. Kolthoff, I. M.; Stricks, W.; Tanaka, N., The Polarographic Prewaves of Cystin (RSSR) and Dithiodiglycolic Acid (TSST) and the Oxidation Potentials of the Systems RSSR-RSH and TSST-TSH. *J. Am. Chem. Soc.* **1955,** *77*, 4739.

49. Birke, R. L.; Mazorra, M., A Study of the Electrochemical Characteristics of some Thiols by Differential Pulse Polarography and other Electrochemical Techniques. *Anal. Chim. Acta* **1980,** *118*, 257.

50. Moaz, R.; Sagiv, J., Penetration-controlled Reactions in Organized Monolayer Assemblies. 1. Aqueous Permanganate Interaction with Monolayer and Multilayer Films of Long-chain Surfactants. *Langmuir* **1987,** *3*, 1034.

51. Lindford, M. R.; Chidsey, C. E. D., Alkyl Monolayers Covalently Bonded to Silicon Surfaces. *J. Am. Chem. Soc.* **1993,** *115*, 12631.

52. Ciampi, S.; Harper, J. B.; Gooding, J. J., Wet Chemical Routes to the Assembly of Organic Monolayers on Silicon Surfaces via the Formation of Si-C Bonds: Surface Preparation, Passivation and Functionalization. *Chem. Soc. Rev.* **2010,** *39*, 2158.

53. Linford, M. R.; Fenter, P.; Eisenberger, P. M.; Chidsey, C. E. D., Alkyl Monolayers on Silicon Prepared from 1-Alkenes and Hydrogen-terminated Silicon. *J. Am. Chem. Soc.* **1995,** *117*, 3145.

54. Bansal, A.; Li, X.; Lauermann, I.; Lewis, N. S.; Yi, S. I.; Weinberg, W. H., Alkylation of Si Surfaces Using a Two-Step Halogenation/Grignard Route. *J. Am. Chem. Soc.* **1996,** *118*, 7225.

55. Scheres, L.; Giesbers, M.; Zuilhof, H., Self-assembly of Organic Monolayers onto Hydrogen-terminated Silicon: 1-Alkynes are Better than 1-Alkenes. *Langmuir* **2010,** *26*, 10924.

56. Scheres, L.; Giesbers, M.; Zuihof, H., Organic Monolayers onto Oxide-Free Silicon with Improved Surface Coverage: Alkynes versus Alkenes. *Langmuir* **2010,** *26*, 4790.

57. Scheres, L.; Arafat, A.; Zuihof, H., Self-Assembly of High-Quality Covalently Bound Organic Monolayers onto Silicon. *Langmuir* **2007,** *23*, 8343.

58. McCreery, R. L.; Bergren, A. J., Progress with Molecular Electronic Junctions: Meeting Experimental Challenges in Design and Fabrication. *Adv. Mater.* **2009,** *21*, 4303.

59. Asanuma, H.; Noguchi, H.; Huang, Y. F.; Uosaki, K.; Yu, H. Z., Probing the Molecular Conformation of Self-Assembled Monolayers at Metal/Semiconductor Interfaces by Vibrational Sum Frequency Generation Spectroscopy. *J. Phys. Chem. C* **2009,** *113*, 21139.

60. Selzer, Y.; Salomon, A.; Cahen, D., Effect of Molecule-Metal Electronic Coupling on Through-bond Hole Tunneling across Metal-organic Monolayer-semiconductor Junctions. *J. Am. Chem. Soc.* **2002,** *124*, 2886.

61. Holmlin, R. E.; Haag, R.; Chabinyc, M. L.; Ismagilov, R. F.; Cohen, A. E.; Terfort, A.; Rampi, M. A.; Whitesides, G. M., Electron Transport through Thin Organic Films in Metal−Insulator−Metal Junctions Based on Self-Assembled Monolayers. *J. Am. Chem. Soc.* **2001,** *123*, 5075.

62. Liu, Y. J.; Yu, H. Z., Alkyl Monolayer-Passivated Metal–Semiconductor Diodes: Molecular Tunability and Electron Transport. *ChemPhysChem* **2002,** *3*, 799.

63. Popoff, R. T. W.; Asanuma, H.; Yu, H. Z., Long-Term Stability and Electrical Performance of Organic Monolayers on Hydrogen-Terminated Silicon. *J. Phys. Chem. C* **2010,** *114*, 10866.

64. Selzer, Y.; Salomon, A.; Cahen, D., The Importance of Chemical Bonding to the Contact for Tunneling through Alkyl Chains. *J. Phys. Chem. B* **2002,** *106*, 10432.

65. Salomon, A.; Böcking, T.; Gooding, J. J.; Cahen, D., How Important Is the Interfacial Chemical Bond for Electron Transport through Alkyl Chain Monolayers? *Nano Lett.* **2006,** *12*, 2873.

66. Tran, E.; Cohen, A. E.; Murray, R. W.; Rampi, M. A.; Whitesides, G. M., Redox Site-Mediated Charge Transport in a Hg−SAM//$Ru(NH_3)_6^{3+/2+}$//SAM−Hg Junction with a Dynamic Interelectrode Separation: Compatibility with Redox Cycling and Electron Hopping Mechanisms. *J. Am. Chem. Soc.* **2009,** *131*, 2141.

67. Hirsch;, A.; Q. Li; Wudl, F., Globe-trotting Hydrogens on the Surface of the Fullerene Compound C60H6(N(CH2CH2).2O6. *Angew. Chem. Int. Ed. Engl.* **1991,** *30*, 1309.

68. Nijhuis, C. A.; Reus, W. F.; Whitesides, G. M., Mechanism of Rectification in Tunneling Junctions Based on Molecules with Asymmetric Potential Drops. *J. Am. Chem. Soc.* **2010,** *132*, 18386.

69. Zwillinger, D., *CRC Standard Mathematical Tables and Formulae*. 31st Ed. ed.; Chapman & Hall/CRC: **2003**.

70. Liu, Y. J.; Yu, H. Z., Alkyl Monolayer Passivated Metal-Semiconductor Diodes: 2: Comparison with Native Silicon Oxide. *ChemPhysChem* **2003,** *4*, 335.

71. Lefenfeld, M.; Baumert, J.; Sloutskin, E.; Kuzmenko, I.; Pershan, P.; Deutsch, M.; Nuckolls, C.; Ocko, B. M., Direct Structural Observation of a Molecular Junction by High-energy X-ray Reflectometry. *Proc. Natl. Acad. Sci. USA* **2006,** *103*, 2541.

72. Ocko, B.; Kraack, H.; Pershan, P.; Sloutskin, E.; Tamam, L.; Deutsch, M., Crystalline Phases of Alkyl-thiol Monolayers on Liquid Mercury. *Phys. Rev. Lett.* **2005,** *94*, 017802.

73. Magnussen, O. M.; Ocko, B. M.; Deutsch, M.; Regan, M. J.; Pershan, P. S.; Abernathy, D.; Grubel, G.; Legrand, J.-F., Self-assembly of Organic Films on a Liquid Metal. *Nature* **1996,** *384*, 250.

74. Kraack, H.; Ocko, B. M.; Pershan, P. S.; Sloutskin, E.; Deutsch, M., Langmuir Films of Normal-alkanes on the Surface of Liquid Mercury. *J. Chem. Phys.* **2003,** *119*, 10339.

75. Dennler, G.; Scharber, M. C.; Brabec, C. J., Polymer-Fullerene Bulk-Heterojunction Solar Cells. *Adv. Mater.* **2009,** *21*, 1323.

76. Suto, S.; Sakanoto, K.; kondo, D.; Wakita, T.; Kimura, A.; Kakizaki, A.; Hu, C. W.; Kasuya, A., Interaction of C60 with Si(111)7×7 and Si(100)2×1 surfaces studied by STM, PES and HREELS: annealing effect. *Surf. Sci.* **1999,** *438*, 242.

77. Cattaruzza, F.; Llanes-Pallas, A.; Marrani, A. G.; Dalchiele, E. A.; Decker, F.; Zanoni, R.; Prato, M.; Bonifazi, D., Redox-active Si(100) Surfaces Covalently Functionalised with [60]Fullerene Conjugates: New Hybrid Materials for Molecular-based Devices. *J. Mater. Chem.* **2008,** *18*, 1570.

78. Sahoo, R. R.; Patnaik, A., Binding of Fullerene C60 to Gold Surface Functionalized by Self-assembled Monolayers of 8-Amino-1-octanethiol: a Structure Elucidation. *J. Colloid Interface Sci.* **2003,** *268*, 43.

79. Zhang, X.; Teplyakov, A. V., Adsorption of C60 Buckminster Fullerenes on an 11-Amino-1-undecene-Covered Si(111) Substrate. *Langmuir* **2008,** *24*, 810.

Appendices

Appendix A. Safe Handling Procedure of "Piranha" Cleaning

1. Chemicals

- Piranha solution (3:1, v/v, concentrated 96% H_2SO_4: 30% H_2O_2) is highly reactive organic materials. Do not breathe the vapors or spill. Work must be carried out in a fume hood.

2. Mandatory Personal Protective Equipment

- Wear a lab coat, close-toed shoes, no shorts and sandals.
- Wear goggles (to protect against vapors or accidently splashes).
- Wear acid safe gear (properly rated gloves, e.g., neoprene gloves).

3. Equipment

- All usage of the cleaning must be recorded in the log book.
- Piranha attacks organic material (e.g., plastics); use only glass, Teflon or stainless steel containers.
- Prepare the minimum quantity you need (all quantities should be < 20 mL).

4. Preparation of Piranha Clean Solution

- Turn on the hot plate, wait until the temperature reaches 90 °C.
- Add a measured volume of H_2SO_4 in to the reaction vessel.
- Cap H_2SO_4 reagent bottle and return bottle to acid storage cabinet.
- Slowly add a measured volume of H_2O_2 to the reaction vessel.
- Cap H_2O_2 reagent bottle and return bottle to refrigerator (The H_2O_2 is added before the etching process because it immediately produces an exothermic reaction with gas (pressure) release. If the H_2O_2 concentration is at 50% or greater, an explosion could occur.)
- Soak your sample into the Piranha solution, slowly put the vessel onto the hot plate.
- Unplug the hot plate when experiment complete or by the end of the day.

5. Waste and Clean up

- Allow Piranha to cool down to room temperature in an open container. Do not fill over lines. DO NOT tightly seal a container with hot Piranha solution, as the vapors generated could cause the container to explode.
- Pour Piranha solution that has cooled to room temperature (this takes~3 hours) into a properly labeled Piranha waste container. Use a glass funnel if necessary. Use a vented cap for Piranha waste bottle.
- Soak all vessels with 18 MΩ water in the hood for 5 minutes. Discard washed solution into Piranha Clean waste container slowly.
- Repeat the above washing procedure at least 2 more times.
- No (cooled down) piranha waste can be left in the hood overnight.

6. First Aid Procedures

- Skin contact: remove contaminated clothing, rinse affected area with water for 10 minutes
- Eye contact: immediately flush eyes with water for 20 minutes
- Ingestion: Do not induce vomiting. Seek immediate medical attention (dial security at 2-4500).
- Inhalation: remove to fresh air. Resuscitate if necessary. Ensure you do not inhale any vapors released from the victim's lungs.

7. Spill Procedures

For cleaning up spills < 2 mL, use the following procedure:

- Soak a paper towel with water and use this soaked towel to mop up the spill.
- Place this paper towel in a larger beaker (at least 500 mL with ~ 300 mL water).
- Repeat this process with a second paper towel. Soak both towels for > 10 min.
- Wring water from the towels and discard in garbage, pour rinse water into the Piranha clean waste bottle.

For cleaning up spills > 2 mL, use the following procedure:

- Use the acid spill kits as instructed in the SFU Lab safety Course on Spill Response.

Appendix B. Safe Handling Procedure of Ammonium Fluoride 40% Solution

1. Chemicals

- Ammonium fluoride solid is white crystal and the solution is clear, colorless liquid that has a slightly sharp, pungent odor. The concentration of ammonium fluoride solution we use is 40% in water, with a pH of around 6.5-7.2. It poses risks on skin, inhalation or ingestion exposure. Therefore, it should be used in a fume hood and appropriate gloves should be weared.

2. SiO_2 Etching Mechanism[1]

- The SiO_2 etch chemistry and reaction mechanisms are summarized as follows.
- The NH_4F is dissociated according to: $NH_4F \rightleftharpoons NH_4^+ + F^-$.
- NH_4F react with SiO_2: $SiO_2 + 6NH_4F \rightleftharpoons SiF_6^{2-} + 2H^+ + 6NH_3 + 2H_2O$.

3. Mandatory Personal Protective Equipment

- Wear a lab coat and close-toed shoes; no shorts and sandals.
- Wear goggles (to protect from vapors and accidental splashes).
- Gloves – wear nitrile gloves inside the long-arm neoprene gloves (outside). Gloves and equipment should be sprayed with either calcium chloride or sodium bicarbonate solution and rinsed with lots of water before being removed from the fume hood.

4. Equipment

- NH_4F can only be used in specific Teflon containers.
- Do not mix up these containers with the ones used for piranha solution.

5. Usage

- Note: NH_4F 40% solution is recommended to be used as the etching agent for silicon wafers.
- Pour enough NH_4F 40% solution to the container. (Depends on the size of the silicon wafer.)
- Stick the tube into the bottom of the container through one of the two holes. Let the other one open to air.
- Open valve 1 first. Then open switch 2 (or 3) (this is when the direction of the valve is parallel to the tube, the gas flows in the direction of arrow) to deoxygenate the NH_4F 40% solution with Ar gas. Position the sash in front of you when bubbling with Ar gas.
- The NH_4F 40% solution should be bubbled with Ar gas for at least 30 min before immersing a silicon wafer into it.
- Lift the tube to just above the surface of NH_4F 40% solution after bubbling with Ar gas.
- Immerse the silicon wafer into NH_4F 40% solution. (Note: The polished side of silicon wafer should face the bottom of the container.)
- Etching the silicon wafer for proper time (Note: It takes around 15 min to obtain H-Si≡.)

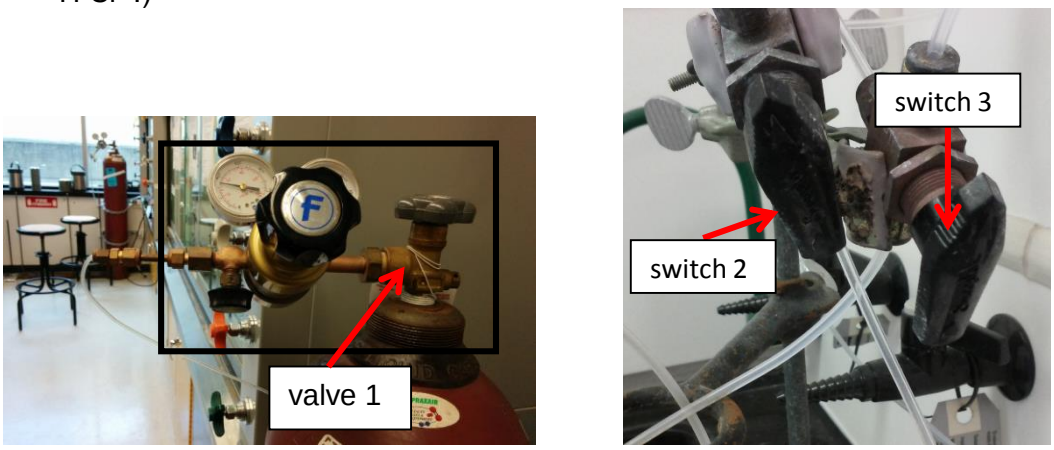

Figure A-1. The pictures for valve 1 and switches 2 and 3.

- Take the silicon wafer out with Teflon tweezers. Close switch 2 (or 3) (the direction of the valve is perpendicular to the tube) first. Then close valve 1.
- Wash the silicon wafer with a trace amount of deionized water.
- Return the bottle to acid storage cabinet (under the fume hood) by the end of the day.

6. Waste

- Pour the used NH_4F solution into the designated waste bottle. Once the bottle is filled to the maximum line, get it disposed of properly by requesting a disposal

request from science store. (http://www.sfu.ca/srs/ehs/research-safety/chemical-safety/protocols-resources/chemical-disposal.html)

- Note: Do NOT pour any other liquid wastes to the designated waste bottle for NH_4F solution! Never use a glass bottle for NH_4F solution!

7. First Aid Procedures

- Skin contact
  - Take off contaminated clothing and shoes immediately.
  - Wash with plenty of water for at least 10 minutes.
  - Immediately apply Calcium Gluconate gel to skin which is stored in the first aid kit beside the door. The gel will turn NH_4F to a white precipitate (CaF_2). Continue to apply Calcium Gluconate gel after the pain has completely subsided for at least 15 minutes. (Note: Apply gel only after washing with water. Continue to apply Calcium Gluconate gel to skin until further medical treatment is available.)
  - Call campus security (2-4500). If need to go to the hospital, take Calcium Gluconate gel with you. Cover area with a dressing soaked in Calcium Gluconate and bind it up tightly with bandage.
  - For severe exposures, Mylanta or 4 effervescent Calcium Gluconate tablets (600 mg) should be taken every 2 hours until the patient is sent to hospital.
- Eye contact
  - Immediately flush eyes at the nearest eyewash for at least 15 minutes while gently lifting the eyelids.
  - Do not use Calcium Gluconate gel.
  - Immediate medical attention is required.
  - Call campus security (2-4500).
- Inhalation
  - In case of accidents of inhalation: move the victim to open areas.
  - Give oxygen or artificial respiration if needed.
  - Mylanta or 4 effervescent Calcium Gluconate tablets (600 mg) should be taken every 2 hours until the patient is sent to hospital.
  - Call campus security (2-4500).
- Ingestion
  - Do not induce vomiting unless directed by medical personnel.
  - Drink warm water and milk to protect mucous linings.
  - Keep body warm.
  - Mylanta or 4 effervescent Calcium Gluconate tablets (600 mg) should be taken every 2 hours until the patient is sent to hospital.
  - Call campus security (2-4500).

8. Spill Control

- Small Spills: Spills less than 50 mL of NH_4F can be considered a small spill. Use the acid spill kit as instructed on Spill Response.
- Large spills: Call campus security and the Environmental Health and Safety office for large spills. Do not attempt to clean these spills.

References

(1) Buhler, J.; Steiner F-P.; Balte, H., Silicon Dioxide Sacrificial Layer Etching in Surface Micromachining. J. Micromech. Microeng. **1997**, *7*, R1.

Appendix C. Electrical Properties for Hg-S-C18|H-Si≡ Junctions: Reproducibility

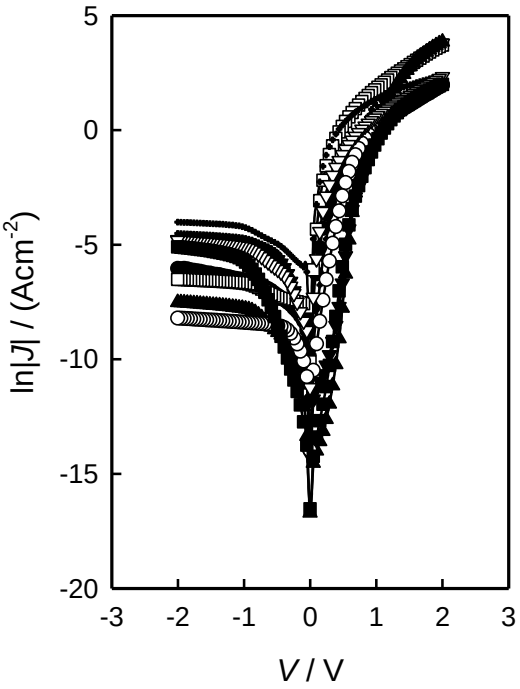

Figure A.2 Current-density vs. voltage (J-V) plots of eight Hg-S-C18|H-Si≡ junctions.

Table A.1 ***Electrical Properties of Hg-S-C18|H-Si≡ Junctions (as prepared)***

	$e\phi_{eff}$ (eV)	η	R
H-S-C18|H-Si≡	0.68±0.04	2.1±0.3	197±40

Appendix D. Electrical Properties for Hg|C12-S-Si≡ Junctions: Reproducibility

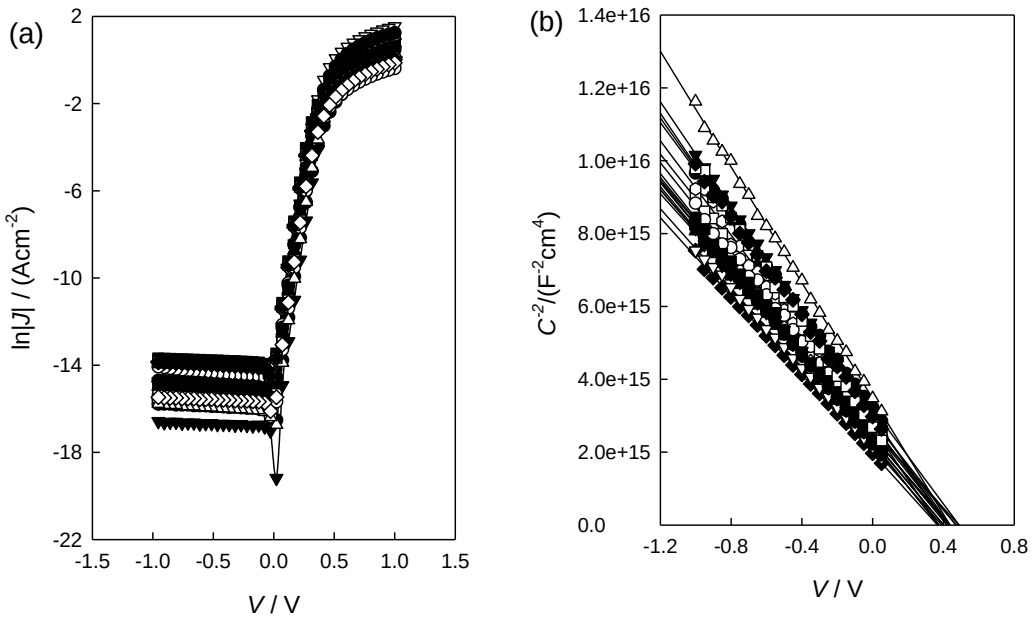

Figure A.3 (a) Current-density vs. voltage (J-V) and (b) capacitance vs. voltage (C-V) plots of sixteen Hg|C12-S-Si≡ junctions.

Table A.2 ***Electrical Properties of Hg|C12-S-Si≡ Junctions (as prepared)***

$R\ (10^6)$	$e\phi_{eff}$ (eV)	η	V_{bi} (eV)	$N_d\ (10^{15}\ cm^{-3})$
5.0±2.1	0.80±0.03	1.04±0.01	0.43±0.05	2.0±0.3